FORUM HOLZBAU INTERNATIONAL

27th International Wood Construction Conference (IHF)
Master Colloquium
Volume III November 30, 2023
Practical experience – Practical application

Content MASTER COLLOQUIUM

Moderation and welcome

Prof. Dr. Sigrist Christophe
Bern University of Applied Sciences
Solothurnstrasse 102
2500 Biel/Bienne, Switzerland

+41 32 344 03 76
christophe.sigrist@bfh.ch

Gertiser Christa
Bern University of Applied Sciences
Solothurnstrasse 102
2500 Biel/Bienne, Switzerland

+41 32 344 02 50
christa.gertiser@bfh.ch

Speakers

Brendel Anna Maria
Technical University of Munich
Arcisstrasse 21
80333 München, Germany

anna-maria@beb-brendel.de

Kramer Lukas
Bern University of Applied Sciences
Solothurnstrasse 102
2500 Biel/Bienne, Switzerland

lukas.kramer@bfh.ch

Lichtblau Leoni
Technical University of Munich
Arcisstrasse 21
80333 München, Germany

leoni@lichtblau.de

Link Pia
Rosenheim Technical University of Applied Sciences
Hochschulstrasse 1
83024 Rosenheim, Germany

pia.link@stud.th-rosenheim.de

Lukas Julian
Univesity Stuttgart
Pfaffenwaldring 7
70569 Stuttgart, Germany

juli.lukas@outlook.de

Selmer Paul
OTH Regensburg
Seybothstrasse 2
93053 Regensburg, Germany

paul.selmer@st.oth-regensburg.de

Behaviour factor for light frame timber shear walls in the context of the second generation of the Eurocode

Lukas Kramer
Bern University of Applied Sciences
School of Architecture, Wood and Civil Engineering
Biel/Bienne, Switzerland

Behaviour factor for light frame timber shear walls in the context of the second generation of the Eurocode

1. Introduction

For the seismic design of timber buildings, force-based design is predominant. Therefore, the behaviour factor q is of great importance in determining the action. In Switzerland dissipative design of light frame timber shear walls (LFTSW) is not interesting from an economic point of view. This is due to a rather low behaviour factor and high overstrength factors compared with other structural types. These high overstrength factors may indicate that the behaviour factor of conventionally designed LFTSW could be increased. Thus, the objective is to determine behaviour factors for different overstrength factors.

The interval between no overstrength factor γ_{RD} / k_{deg} = 1.0 and the required overstrength factor to ensure dissipative failure with a high enough probability is of particular interest. From this, a new dissipative light design method could be developed which can be designed with a higher behaviour factor than 1.5. In the dissipative design, the partial safety factor γ_M is specified as 1.0. However, the factor k_{deg} = 0.8 must be applied to the resistance of the dissipative element. Therefore, the ratio of γ_{RD} and k_{deg} best represents the change in the ratio of the resistance of the individual elements of a LFTSW. Accordingly, γ_{RD} / k_{deg} is used for ease of understanding. The investigations are based on the draft of the second generation of the Eurocode from July 2022.

2. Methods

In literature multiple procedures were suggested for the evaluation of behaviour factors [1, 2]. The nonlinear static analysis (NLSA) is chosen for the evaluation of the behaviour factor. As many different variants were evaluated, numerical investigations com with far smaller material and financial costs. The NLSA have the advantage of comparing two design methods in prEN 1998-1-1:2022 [3] as well as having shorter calculation times when compared to nonlinear dynamic analysis (NLDA). Furthermore, NLSA is a clear procedure when compared to NLDA. Thereby, the behaviour factor is determined by matching the force-based design with the displacement-based design. A structure is designed according to force-based design with a behaviour factor q = 1. Through displacement-based design the maximal compatible spectrum (MCS) is determined. The increase in the acceleration spectrum corresponds to the applicable behaviour factor.

2.1. Nonlinear Static Analysis

The displacement-based design in the Eurocode is based on the N2 method. The N2 method is a nonlinear static design method. It was developed to represent the behaviour of the building better than linear elastic static methods. At the same time, the effort should remain low [4]. For the implementation in EN 1998-1:2010 [5] as well as in prEN 1998-1-1:2022 [3], minor adaptations have been made. This concerns the adjustment of the elastic displacement to account for the shape of the inelastic.

A further adjustment of the aforementioned adjustment is given for LFTSW for medium to low seismicity [6]. The stiffness for the evaluation of the fundamental period is defined by the yield point. In the prEN 1998-1-1:2022 [3] the definition of the yield point is not defined trough an evaluation procedure. Thus for LFTSW the yield force is defined as the design resistance for very short actions based on the experimental results of Preile and Geiser 2018; Kramer and Geiser 2021; Peinhopf 2022 [7–9] and Schweizer 2022 [10].

2.2. Maximal compatible spectrum

The MCS is needed for the calculation of the behaviour factor. For the determination of the MCS, the acceleration is linearly scaled by a factor α_{MCS} until the utilization of the displacement-based verification is 100%. The behaviour factor *q* corresponds to α_{MCS} as it is the increase of the acceleration spectrum.

$$S_{e,MCS} = \alpha_{MCS} \cdot S_e \tag{1}$$

$$S_{d,MCS} = S_{e,MCS} \left(\frac{T_1}{2\pi} \right)^2 \tag{2}$$

2.3. Light Frame Timber Shear Walls

For all investigations a single wall with length 2.5 m and height 2.8 m is the basis. The sheathing is of OSB/3 and has a thickness of 18 mm. The frame elements were made of GL24h whilst the anchorage is made of S355. The tension anchorage is located at the neutral axis of the edge studs. No fasteners were explicitly considered for the anchorage.

For the connection between sheathing and frame two types of nails were used. Both nails have a partial ring shank, a diameter of 3.1 mm and a length of 90 mm. The first type is made of normal steel (NN) and the second type is a seismic nail made of stainless steel (SN). The NN reach a cyclic ductility of 4, the SN reaches a cyclic ductility of 6 according to the EN 12512 [11] in [9, 10].

For the calculation of the force-displacement curves, the displacement components are calculated following the equivalent member method as described in the state of the art document Mehrgeschossige erdbebengerechte Holzbauten [12]. The only non-linear element taken into account are the fasteners of the sheathing to framing. Therefore, the stiffness of the fastener is used as a function of the acting force.

The force-displacement curve of the nails is characterized by the model of Dolan and Foschi [13]. For the characterization tests were performed according to the EN 12512 [11]. The evaluation was done according to prEN 1998-1-2:2022 [14]. For the characterization the Load Envelope Curve 1 (LEC1) is used.

2.4. Overview of the procedure for determining the behaviour factor

The LFTSW is designed with force based design considering a behaviour factor q = 1.0 so that all elements are verified with a utilization of 100%. The next step is the calculation of the pushover-curve. The pushover-curve is idealized with a bi- or trilinear curve defined by the yield point, the maximal force and if different to the maximal force the ultimate displacement. The MCS is determined and with this the applicable behaviour factor as described in 2.2. The overstrength part q_s is determined by equation (3). With the overstrength part given, the ductility part q_d can be determined by equation (4).

$$q = \alpha_{MCS} \tag{3}$$

$$q_s = \frac{F_{SD}}{F_d} \tag{4}$$

$$q_d = \frac{q}{q_s} \tag{5}$$

2.5. Boundary conditions

Soil class D and earthquake zone Z3b of the SIA 261 [15] are used for all investigations. The spectra in SIA 261 [15] reflect the latest insights into the seismic hazard in Switzerland. At the same time the spectra were only slightly changed in comparison to the prEN 1998-1-1:2022 [3] and the spectra remain very similar [16].

A probabilistic model is determined for all material properties, details can be found in Kramer 2023 [17]. From these, the properties for 1000 walls were sampled. This results in 1000 behaviour factors for each of the variants described below The resistance for displacement based design according to Annex L in the prEN 1998-1-2:2022 [14] is defined to be the 16% fractile.. Thus, the allowable behaviour factor corresponds to the empirical 16% fractile value.

2.6. Influence of the applied overstrength factor

As stated in the introduction, a possible new dissipative light design method with an increased behavior factor compared with ductility class 1 (DC1) with small overstrength factors were of interest. In order to find an interesting overstrength factors γ_{Rd} / k_{deg} between 1.0 and 2.8 in 0.2 steps were investigated for both types of nails.

2.7. Influence of the design resistance of the fasteners

In the second generation of the Eurocode 5 [18] the design resistance of dowel-type fasteners increased in comparison with the first generation of the Eurocode 5 [19]. For the SN fasteners, the influence this change in design resistance is determined for different overstrength factors γ_{Rd} / k_{deg}.

2.8. Determination of the sensitivity factors

So far, the focus was on the influence of multiple factors in the code. Besides the design factors, the importance of different elements of the LFTSW on the behaviour factor is of interest as well. This information helps to prioritize these in the production or construction site inspection. Screening methods were used for this investigation. Specifically the sensitivity factors according to Cotter [20] as well as Morris [21–23] were determined.

3. Results and Discussion

In this section the allowable behaviour factor for each investigated variant is displayed and discussed.

3.1. Influence of the applied overstrength factor

For the design according to the dissipative structural behaviour, the behaviour factor shows two distinct zones. For overstrength factors between 1.0 and 1.4 an increase of the behaviour factor is evident. The maximal behaviour factor for the SN nails is just larger than 2.0. The failure of the dissipative element is not ensured with a high enough probability. Thus, only walls which failed in non-dissipative elements were used for the definition of the allowable behaviour factor. This changes with an overstrength factor of at least 1.6 and the behaviour factor is significantly higher. This is true for both fastener types. For DC3, the overstrength part q_s is confirmed, the ductility part q_d = 2.4 in the prEN 1998-1-2:2022 [14] is not confirmed as it is larger than the evaluated 2.2. The results are shown in Figure 1.

The behaviour factor according to the non-dissipative structural behaviour is between 1.7 and 2.0, containing the overstrength part q_s and the ductility part q_d. Thus the combination of both parts leads to a confirmation of the defined behaviour factor q = 1.5 in the prEN 1998-1-2:2022 [14].

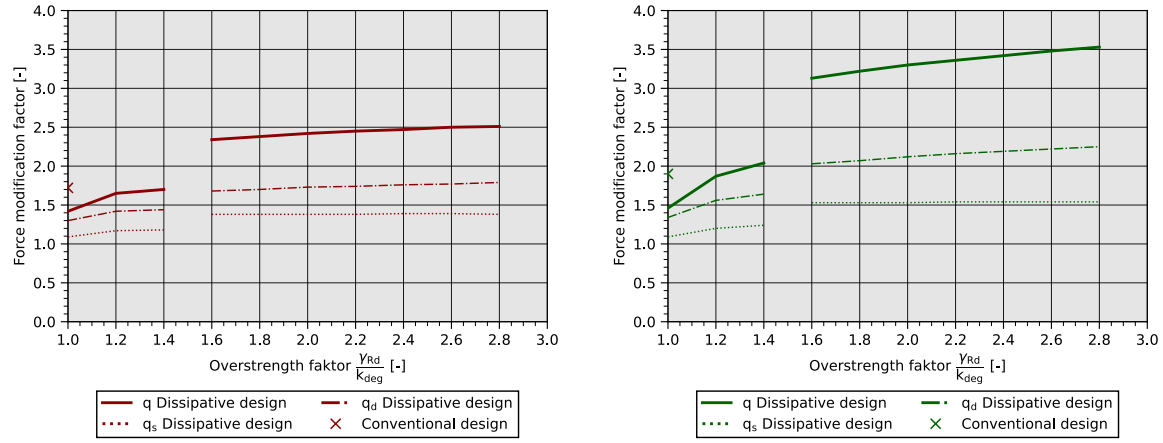

(a) (b)

Figure 1 Behaviour factor for different overstrength factors. (a) NN, (b) SN

3.2. Influence of the design resistance of the fasteners

With dissipative design, the behaviour factors are almost always higher over the range of the overstrength factor with a lower design resistance. The differences are only due to a higher overstrength part q_s. However, this higher overstrength part q_s of the behaviour factor can only be achieved with a higher overstrength factor γ_{Rd} / k_{deg}. The results are shown in Figure 2.

In non-dissipative design, the behaviour factor increases with the increase in the design resistance by 0.2.

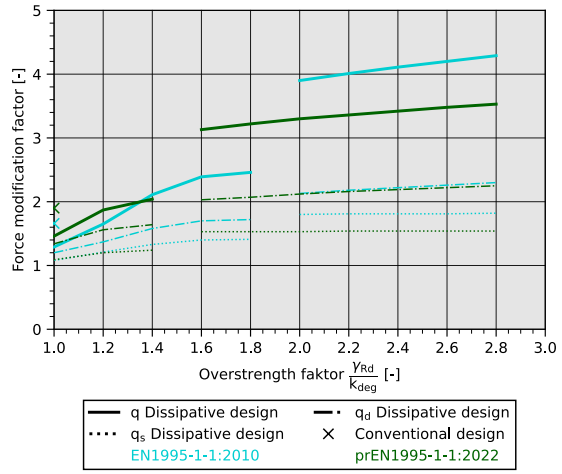

Figure 2 Behaviour factor for different overstrength factors and different design resistances of the dissipative element

3.3. Sensitivity factors

The sensitivity factors are evaluated in order to determine the most important elements of the LFTSW. The screening methods used do not allow for comparison of the absolute values of the sensitivity factors. Thus, only the ranking itself should be considered.

In the non-dissipative designed LFTSW the edge studs and the sheathing are most important. This is evident in the Figure 3.

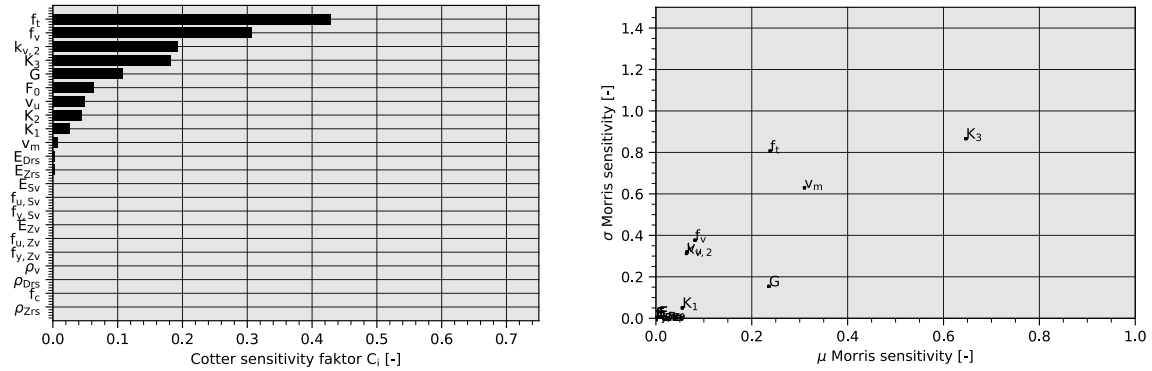

(a) (b)

Figure 3 Sensitivity factors of non-dissipative designed LFTSW (a) Sensitivity factor according to Cotter (b) Sensitivity factors according to Morris

For the dissipative designed LFTSW the fastener is the most important element. This is evident in the Figure 4.

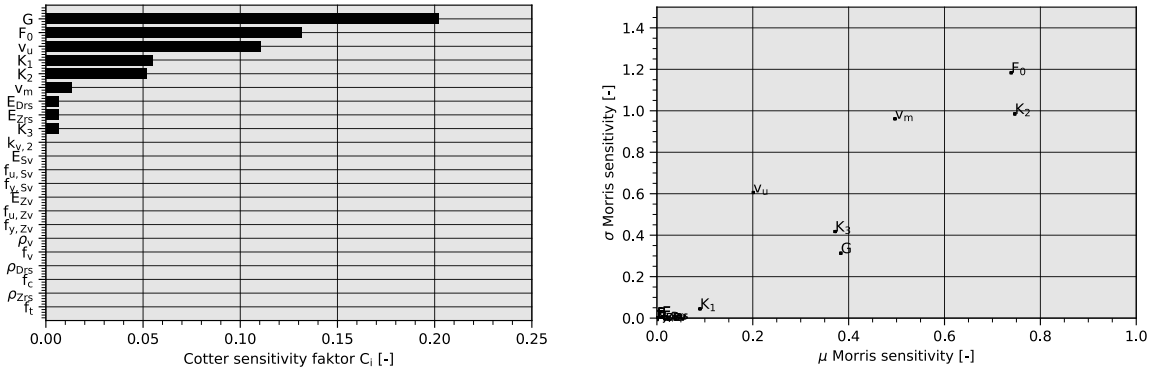

(a) (b)

Figure 4 Sensitivity factors of dissipative designed LFTSW with γ_{Rd}/k_{deg} = 2,0 (a) Sensitivity factor according to Cotter (b) Sensitivity factors according to Morris

4. Conclusion

An increased behaviour factor of 2.0 might be possible with a smaller overstrength factor of 1.4 compared with the needed overstrength factor of 1.6. But from an economic point of view this is not interesting, as with an increase of only 0.2 in the overstrength factor the behaviour factor increases by more than 1 point. This goes with the same effort for the engineering as well as the production.

For the design according to the non-dissipative structural behaviour in DC1, a utilization of the of the fastener design resistance smaller than 100% is less conservative with regard to the behaviour factor.

For non-dissipative LFTSW, the grade and cross section of the edge studs and the sheathing should be emphasized in the inspection. For dissipative designed LFTSW, the type of fastener and the fastener spacing should be prioritized in the inspection.

5. Acknowledgement

This work is part of a project to developpe a method for modelling, design and construction of light frame timber shear walls with large openings, which is financed by Holzbau Schweiz, the Swiss Timber Engineers, Ancotech and the FOEN's Wood Action Plan 2021 – 2026. Furthermore, a big thanks goes to the advisor Prof. Martin Geiser for the continuous support.

6. References

[1] A. Ceccotti, M. Massari, and L. Pozza, «Procedures for seismic characterization of traditional and modern wooden building types,» 2016. [Online]. Available: http://ijqr.net/journal/v10-n1/2.pdf

[2] D. Vamvatsikos *et al.,* «A risk-consistent approach to determine EN1998 behaviour factors for lateral load resisting systems,» vol. 131, 2020.

[3] *Eurocode_8: Auslegung von Bauwerken gegen Erdbeben_- Teil_1: Grundlagen, Erdbebeneinwirkungen und Regeln für Hochbauten*, prEN 1998-1-1:2022, EN, Brüssel.

[4] P. Fajfar and P. Gaspersic, «The N2 method for the seismic damage analysis of rc buildings,» *Earthquake Engineering & Structural Dynamics*, vol. 25, no. 1, pp. 31–46, 1996, doi: 10.1002/(SICI)1096-9845(199601)25:1<31::AID-EQE534>3.0.CO;2-V.

[5] *EN 1998-1:2010-12, Eurocode_8: Auslegung von Bauwerken gegen Erdbeben_- Teil_1: Grundlagen, Erdbebeneinwirkungen und Regeln für Hochbauten: Deutsche Fassung EN_1998-1:2004_+ AC:2009*, EN 1998-1:2010, EN.

[6] P. Mergos and K. Beyer, «Displacement-Based Seismic Design of Symmetric Single-Storey Wood-Frame Buildings with the Aid of N2 Method,» *Front. Built Environ.*, vol. 1, p. 10, 2015, doi: 10.3389/fbuil.2015.00010.

[7] K. Preile and M. Geiser, «Propriétés dynamiques des bâtiments à ossature bois - Rapport de travail sur l'étape de travail AP2 - Détermination de la rigidité des matériaux et assemblages,» 2018.

[8] L. Kramer and M. Geiser, «Tragverhalten mehrgeschossiger Holzbau: Tragverhalten und adaptive Steifigkeit von Holzrahmenbauwänden für erdbebengerechte Gebäudeaussteifung im mehrgeschossigen Holzbau,» 2021.

[9] G. Peinhopf, «Steifigkeit, Tragwiderstand und Duktilität genagelter, geklammerter OSB-Holzverbindungen sowie genagelter GFP-Holzverbindungen,» Berner Fachhochschule AHB, Biel, 2022.

[10] R. Schweizer, «Einfluss der Stahlqualität und des Nageltyps auf die Duktilität von OSB-Holz-Nagelverbindungen,» BSc Thesis, Berner Fachhochschule AHB, Biel, 2022.

[11] *EN 12512:2005-12, Holzbauwerke_- Prüfverfahren_- Zyklische Prüfungen von Anschlüssen mit mechanischen Verbindungsmitteln; Deutsche Fassung EN_12512:2001_+ A1:2005*, EN 12512, SN; EN, 2005.

[12] R. Brunner, P. Jung, R. Steiger, T. Wenk, and N. Wirz, «Erdbebengerechte mehrgeschossige Holzbauten,» 2010.

[13] J. D. Dolan and R. O. Foschi, «Structural Analysis Model for Static Loads on Timber Shear Walls,» *J. Struct. Eng.*, vol. 117, no. 3, pp. 851–861, 1991, doi: 10.1061/(ASCE)0733-9445(1991)117:3(851).

[14] *Eurocode_8: Auslegung von Bauwerken gegen Erdbeben_- Teil_2: Hochbauten*, prEN 1998-1-2:2022, EN, Brüssel.

[15] *Einwirkungen auf Tragwerke*, SIA 261:2020, SIA, Zürich.

[16] B. Duvernay, D. Fäh, M. Koller, and T. Wenk, *Aktualisierung der Erdbebeneinwirkungen der Norm SIA 261:2014: Grundlagenbericht*, 2019.

[17] L. Kramer, «Verhlatensbeiwert q von Holzrahmenbauwandscheiben im Kontext der zweiten Generation des Eurocodes,» Masterthesis, Berner Fachhochschule AHB, Biel, 2023.

[18] *Eurocode 5: Bemessung und Kontruktion von Holzbauten - Allgemeine Regeln und Regeln für den Hochbau - Teil 1-1: Allgemeines*, prEN 1995-1-1:2022, EN, Brüssel.

[19] *DIN EN 1995-1-1:2010-12, Eurocode 5: Bemessung und Konstruktion von Holzbauten - Teil 1-1: Allgemeines_- Allgemeine Regeln und Regeln für den Hochbau;: Deutsche Fassung EN 1995-1-1:2004 + AC:2006 + A1;2008*, EN 1995-1-1:2010, EN, Brüssel, 2010.

[20] G. Qian, M. Massenzio, D. Brizard, and M. Ichchou, «Sensitivity analysis of complex engineering systems: Approaches study and their application to vehicle restraint system crash simulation,» *Reliability Engineering & System Safety*, vol. 187, pp. 110–118, 2019, doi: 10.1016/j.ress.2018.07.027.

[21] M. D. Morris, «Factorial Sampling Plans for Preliminary Computational Experiments,» *Technometrics*, no. 33, pp. 161–174, 1991.

[22] F. Campolongo, J. Cariboni, and A. Saltelli, «An effective screening design for sensitivity analysis of large models,» *Environmental Modelling & Software*, vol. 22, no. 10, pp. 1509–1518, 2007, doi: 10.1016/j.envsoft.2006.10.004.

[23] S. Kucherenko, M. Rodriguez-Fernandez, C. Pantelides, and N. Shah, «Monte Carlo evaluation of derivative-based global sensitivity measures,» *Reliability Engineering & System Safety*, vol. 94, no. 7, pp. 1135–1148, 2009, doi: 10.1016/j.ress.2008.05.006.

Investigations of lateral torsional buckling of timber beams under combined bending and compression

Julian Lukas
Chair for Timber Structures and Building Construction
Technical University of Munich
Munich, Germany

Janusch Töpler
Institute of Structural Design
University of Stuttgart
Stuttgart, Germany

Prof. Dr.-Ing. Ulrike Kuhlmann
Institute of Structural Design
University of Stuttgart
Stuttgart, Germany

Investigations of lateral torsional buckling of timber beams under combined bending and compression

1. Introduction

The increasing importance of saving and storing CO2 emissions leads to an increasing demand for wood as a construction material. Particularly in the case of long-span structures, the desire for wooden beams that are as slender as possible is growing. These are usually loaded by a combination of bending and axial force (*N-M* interaction). However, with increasing slenderness, the risk of stability failure also increases. Depending on the type of loading, this results in in-plane buckling or lateral torsional buckling (LTB) of timber beam-columns (see Figure 1).

Due to the complexity of the stability behaviour, LTB is still a much discussed topic with many remaining challenges. Analytical investigations by *Abeysekera et al.* [1], *Hörsting* [7] and *Töpler & Kuhlmann* [12] show that the design rules according to the currently valid standard EN 1995-1-1:2004 [6] provide conservative results and are based on a mechanically incorrect combination of axial force and bending [1].

In this paper, the analytical model for the geometrically and materially non-linear analysis of beams at risk of LTB according to *Hörsting* [7] and *Töpler & Kuhlmann* [12] is extended. The deformation analysis of beams due to geometric and material non-linear behaviour is further developed. When considering the size effect, the assumption of a constant stress course over the length is modified so that a variable course of stresses over length, width and height is taken into account. The calculation of the analytical equations is implemented in the programming language *Python* (v3.10.6). The results of the extended analytical model are compared with current design rules. In combination with numerical and experimental investigations, it can be used to optimise the existing design rules to enable more economic results for *N-M* interaction.

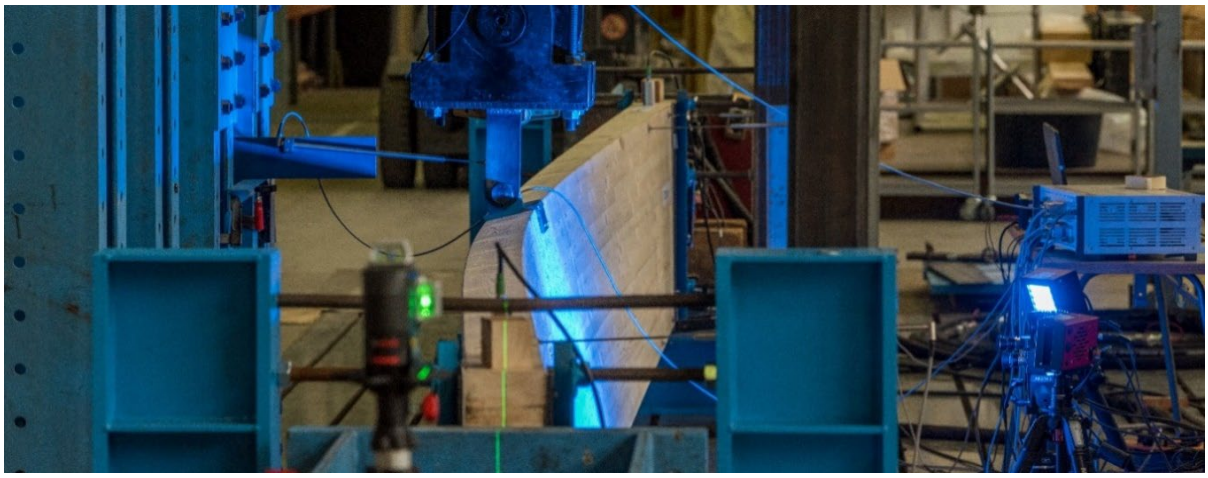

Figure 1: LTB test on a glulam beam with dimensions 8000 x 720 x 120 mm³ [13].

2. State of the art

Generally, stability behaviour can be divided into three phenomena [12]. First, the geometrically nonlinear behaviour describes excessive deformations and associated additional forces (see Section 3.2). Second, materially nonlinear behaviour considers the plasticising in the compression zone of the cross-section due to lower compressive than tensile strength in bending (see Section 3.3). Third, the size effect takes into account the influence of material scattering (see Section 3.4). An analytical model was developed by *Hörsting* [7] by combining all three phenomena. This model can determine the load-bearing capacity

of rectangular imperfection-sensitive timber beams under N_x-M_y loading. The size effect is considered using *Weibull*-theory [15]. Therefore, a constant bending moment is assumed over the beam length [7]. An ideal bilinear elasto-plastic material behaviour for compression parallel to the fibre was considered. Since the geometric non-linear material behaviour is significantly influenced by the stiffness of the beam (see Section 3.2) *Töpler & Kuhlmann* [12] extended the model according to *Hörsting* [7] in such a way that a decrease in stiffness due to plasticising is taken into account when determining the internal forces. The analytical model is described in Section 3.

The European standards EN 1995-1-1:2004 [6] and prEN 1995-1-1:2023 [10] describe two procedures for the design of timber members at risk of LTB. On the one hand, the design verification can be carried out with stresses computed according to second order theory (T2O). Up to now, EN 1995-1-1:2004 [6] has allowed design verification using T2O, but no explicit recommendations on the procedure are given. With prEN 1995-1-1:2023 [10], formulas and recommendations on the application of T2O are given for the first time. On the other hand, design verification can be carried out with the help of the effective length method (ELM), which provides structural engineers with simplified design formulas. For the case of the LTB with *N-M* interaction, the reduction factors for the axial stress k_c and the bending stress k_m are combined. Further information on the derivation of the reduction factors can be found in [8] and [13].

To evaluate the load-bearing behaviour of combined *N-M* beams, *Töpler & Kuhlmann* [13] carried out 19 full scale LTB tests on glulam beams. The experimental results were used for validation of a numerical model. A design approach for a combined *N-M* loading is being developed from the results of the numerical and experimental investigations.

3. Analytical model

3.1. General

The developed extension of the analytical model of *Hörsting* [7] and *Töpler & Kuhlmann* [12] is described in the following. First, the equations for considering the geometrically nonlinear behaviour are given. Then the effect of plasticising on the load-bearing capacity and deformation behaviour is described. Then a method is presented to consider variable course of stresses over length, width and height in the size effect. Finally, the calculation procedure for the load-bearing capacity is explained. The basic assumption is a rectangular single-span beam with fork bearings according to Figure 2. The beam can be loaded by a constant bending moment, point load at midspan or line load. In addition, an axial force acts. Further assumptions for the derivation of the following equations see *Hörsting* [7]. To achieve short calculation times, solving the equations is carried out with *Python* using the packages *Numpy* and *Scipy*.

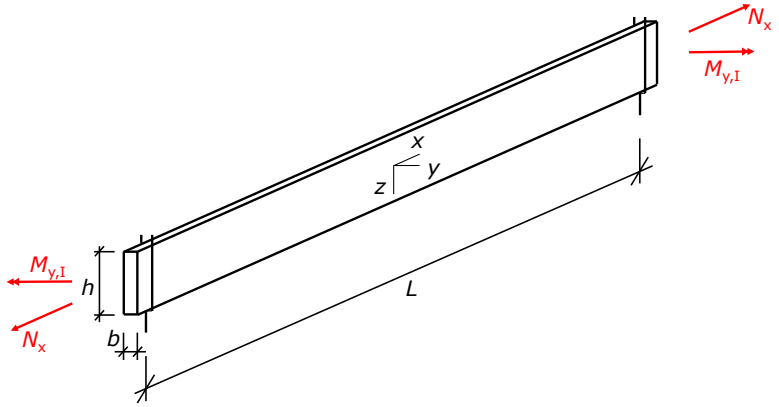

Figure 2: Three-dimensional structural system of a single span beam with fork bearings [12].

3.2. Geometrical non-linear behaviour

The internal forces according to T2O are determined according to the well-known equations according to *Hörsting* [7] and *Töpler & Kuhlmann* [12].

$$M_{\mathrm{y,II}} = \frac{M_{\mathrm{y,I}} \cdot \left(1 + \alpha_{\mathrm{c,y}} \cdot \delta\right) - N_{\mathrm{x}} \cdot e_{\mathrm{z}}}{1 - \alpha_{\mathrm{c,y}}} \tag{3.1}$$

$$M_{\mathrm{z,II}} = \frac{\left(-N_{\mathrm{x}} + \frac{M_{\mathrm{y,I}}^2}{GI_{\mathrm{x}}}\right) \cdot e_{\mathrm{y}} + M_{\mathrm{y,I}} \cdot e_{\vartheta}}{1 - \alpha_{\mathrm{c,z}} - \alpha_{\mathrm{m}}^2} \tag{3.2}$$

with $\alpha_{\mathrm{m}} = \frac{M_{\mathrm{y,I}}}{M_{\mathrm{y,crit}}}$

$M_{\mathrm{y,crit}} = \frac{\pi}{L_{\mathrm{m,ef}}} \cdot \sqrt{GI_{\mathrm{x}} \cdot EI_{\mathrm{z}}}$

$\alpha_{\mathrm{c,y/z}} = \frac{N_{\mathrm{x}}}{N_{\mathrm{crit,y/z}}}$

$N_{\mathrm{crit,y/z}} = -\frac{\pi^2 EI_{\mathrm{y/z}}}{L_{\mathrm{c,y/z,ef}}^2}$

$M_{\mathrm{y/z,I}}$	Applied bending moment around y/z axis (Figure 2)
δ	Dischinger correction factor, prEN 1995-1-1:2023 [10]
E	Modulus of elasticity (MOE) parallel to the grain
G	Shear modulus parallel to the grain
$I_{\mathrm{x/y/z}}$	Moments of inertia according to Eq. (3.9) - (3.11)
$L_{\mathrm{m,ef}}$	Effective length under bending
$L_{\mathrm{c,y/z,ef}}$	Effective length under axial force
$e_{\mathrm{y/z/\vartheta}}$	Equivalent imperfections (Figure 3)

3.3. Material non-linear behaviour

The model according to *Hörsting* [7] is used to determine the load-bearing capacity of a rectangular cross-section. The elasto-plastic material behaviour is simplified by an idealised bilinear stress-strain relationship (see Figure 4). Figure 5 shows an example of the elastic and elasto-plastic stress curve over the cross-section with *N-M* interaction.

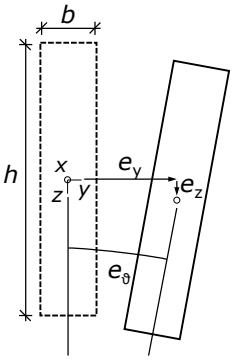

Figure 3: Cross-section position and imperfections in the center of the beam [12].

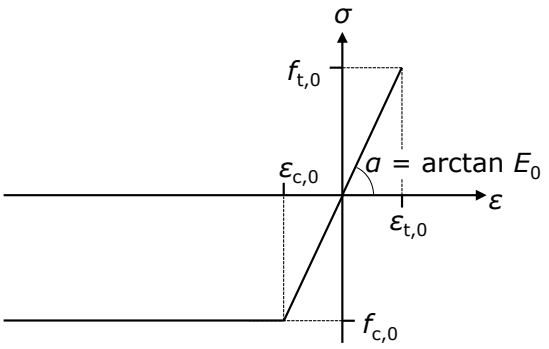

Figure 4: Idealised, bilinear material behaviour of wood parallel to the grain [12].

Depending on the curvatures around the y and z axis the strain over the cross-section can be described with Equation (3.3).

$$\varepsilon(y,z) = \kappa_{\mathrm{y}} \cdot \left(z - \frac{h}{2}\right) + \kappa_{\mathrm{z}} \cdot \left(y - \frac{b}{2}\right) + \varepsilon_{\mathrm{t,0}} \tag{3.3}$$

The corresponding stresses can be calculated according to Equation (3.4).

$$\sigma(y,z) = E \cdot \left[\varepsilon(y,z) + \langle -\left(\varepsilon(y,z) - \varepsilon_{\mathrm{c,0}}\right)\rangle\right] \tag{3.4}$$

el *el-pl*

with	ε	Strain in x direction
	$\varepsilon_{t,0} = f_{t,0}/E$	Elastic tensile strain (see Figure 5)
	$\varepsilon_{c,0} = f_{c,0}/E$	Elastic compressive strain (see Figure 5)
	σ	Stress in x direction
	$\kappa_{y/z}$	Curvature around y and z axis (see Figure 5)
	b/h	Cross-section width and height
	$\langle\ \rangle$	Macaulay brackets

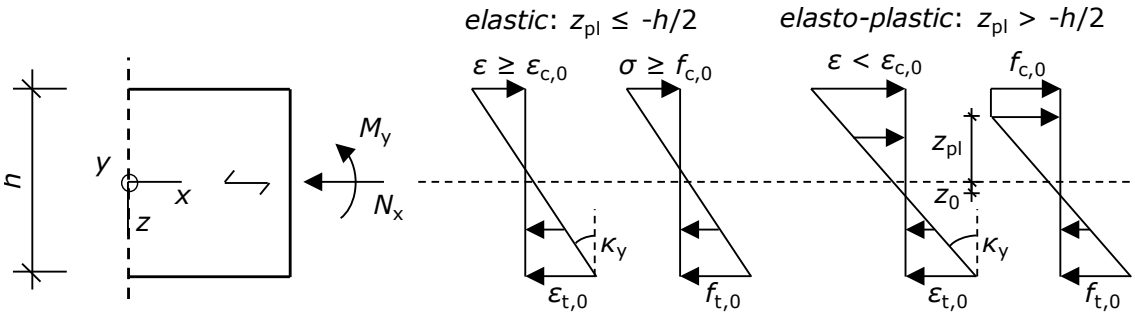

Figure 5: El. and el.-plastic strain and stress curve for M_y-N_x interaction for bilinear material behaviour [7].

When the maximum compressive strength $f_{c,0}$ is exceeded in the compression zone, the cross-section begins to plasticise. The transition between elastic and elasto-plastic behaviour can be described by a line g_{pl}, see Figure 6. A total of five different cases can be distinguished depending on the shape of the plasticised area (see Figure 6). For case no. 1 the line g_{pl} lies outside the cross-section and a purely elastic behaviour occurs. Cases no. 2 to 5 show a plasticised area in the cross-section and thus behave elasto-plastic. *Hörsting* [7] determines the cross-sectional load-bearing capacities of beams $N_{x,R}$, $M_{y,R}$ and $M_{z,R}$ by integrating the stresses according to Equation (3.4) across the cross-section. Considering g_{pl} as integration limit the load-bearing capacities can be derived from Equations (3.5) - (3.7). Due to the complexity of the integration, the derivation is not described in detail, instead see [7], [8], [12].

$$N_{x,R} = \int_{-h/2}^{h/2}\int_{-b/2}^{b/2} \sigma(y,z)\, dy\, dz \tag{3.5}$$

$$M_{y,R} = \int_{-h/2}^{h/2}\int_{-b/2}^{b/2} z \cdot \sigma(y,z)\, dy\, dz \tag{3.6}$$

$$M_{y,R} = \int_{-h/2}^{h/2}\int_{-b/2}^{b/2} y \cdot \sigma(y,z)\, dy\, dz \tag{3.7}$$

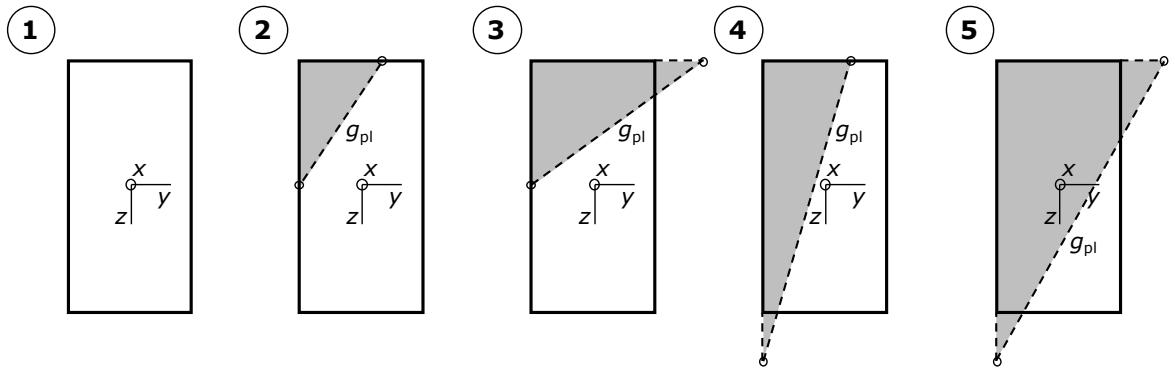

Figure 6: Position of the plastic baseline for biaxial bending M_y – M_z and axial force N_x [12].
Grey: Plasticized cross-section.

The maximum load-bearing capacity is reached when the cross-section is either fully plasticised or the tensile strength in bending, referred to as $f_{t,0}$, is reached. The tensile strength in bending is equal to the bending strength f_m according to EN 14080:2013 [5].
The strain continues to increase in the plasticised area while the stress remains at the level of the maximum compressive strength $f_{c,o}$ (see Figure 4). This causes MOE to become

zero and any cross-sectional stiffness of the plasticised area is lost. When stiffnesses decrease, internal forces according to Equations (3.1) - (3.2) increase [12]. To account for this loss of stiffness, cross-sectional properties are determined, neglecting the plasticised area. According to *Petersen* [9], the cross-sectional values of a polygon can be determined using Equations (3.8) - (3.11).

$$A = \frac{1}{2} \cdot \sum_{i=1}^{n-1} (y_i \cdot z_{i+1} - y_{i+1} \cdot z_i) \tag{3.8}$$

$$I_y = \frac{1}{12} \cdot \sum_{i=1}^{n-1} (y_i \cdot z_{i+1} - y_{i+1} \cdot z_i) \cdot [(z_i \cdot z_{i+1})^2 - z_i \cdot z_{i+1}] \tag{3.9}$$

$$I_z = \frac{1}{12} \cdot \sum_{i=1}^{n-1} (y_i \cdot z_{i+1} - y_{i+1} \cdot z_i) \cdot [(y_i \cdot y_{i+1})^2 - y_i \cdot y_{i+1}] \tag{3.10}$$

$$I_x = \frac{A^4}{4\pi^2 (I_y + I_z)} \tag{3.11}$$

with n Number of corner points of a polygon (first and last entry coincide)

y_i/z_i y/z coordinate at corner point i

The loss of cross-sectional stiffness also affects the deformation behaviour of a beam. However, this only applies to the areas in the beam with a plasticised cross-section. Therefore, a timber beam can be divided into a section with elastic material behaviour of length L_{el} and another section with elasto-plastic material behaviour of length $L_{el\text{-}pl}$ (see Figure 7). The position of the two sections results from the intersection of the acting internal forces according to T2O $M_{y/z,II}$ and the elastic cross-section resistance $M_{y/z,el,R}$ according to a linear strain interaction, see Equation (3.12).

$$-\frac{N_x}{A} + \frac{M_{y,II}}{W_y} + \frac{M_{z,II}}{W_z} = f_{c,0} \tag{3.12}$$

Simplified, the minimum bending stiffness at midspan is assumed for the entire elasto-plastic range. This assumption is on the safe side and allows a simple deformation calculation. The deformation at midspan can be determined by numerical integration. A more detailed description of the calculation of the deflection can be found in [8]. The influence of the varying bending stiffness on Equations (3.1) - (3.2) are currently under development.

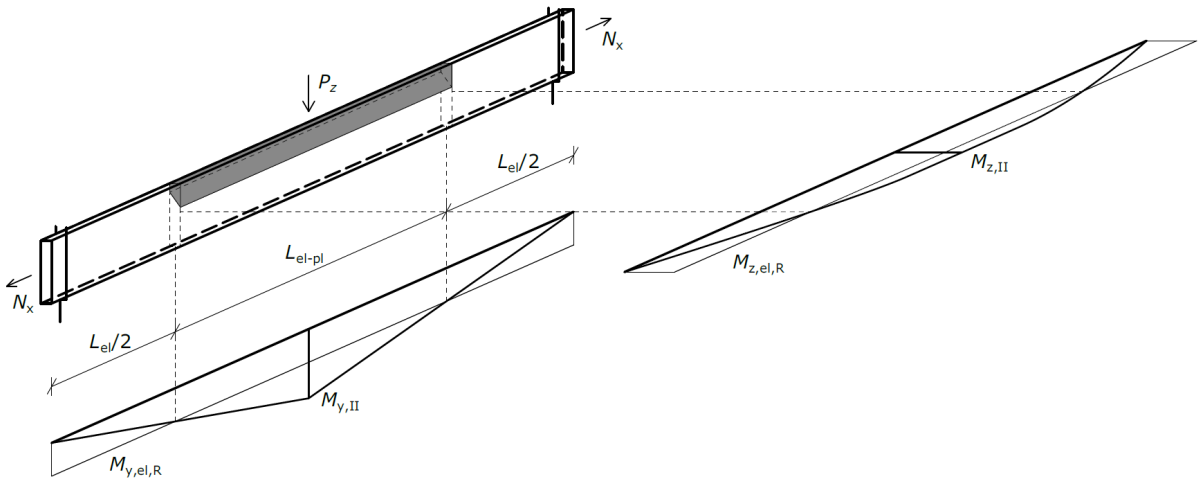

Figure 7: Timber beam divided into an elastic and elasto-plastic area for a point load at midspan. Grey: Plasticized cross-section.

3.4. Size effect

The size effect is an area of extensive research in timber construction such as [2] and [11]. The analytical models according to *Hörsting* [7] and *Töpler & Kuhlmann* [12] consider the size effect according to the *Weibull*-theory [15]. A 2-parametric *Weibull* distribution

with constants m and σ_0 according to [8], [12] is chosen. According to *Hörsting* [7] and *Töpler & Kuhlmann* [12], the calculation approach is based on the assumption that an axial force and constant bending moment exist over the entire length of the beam. However, significant deviations from such an internal force distribution occur when applying a concentrated load or a line load. To take into account the size effect for a variable internal force distribution, the beam can be divided into numerous sections. Since the internal forces according to T2O are known at each point in the beam, the curvatures $\kappa_{y/z}$ and the maximum tensile strain $\varepsilon_{t,0}$ in the beam can be calculated by solving a non-linear system of Equations (3.5) - (3.7). Depending on the location of the neutral axis, the failure probability S can be determined with the factor R in any section of the beam according to the known equation by *Hörsting* [7], see Equations (3.13) - (3.15). The reference cross-section dimensions L_0, b_0 and h_0 must be taken into account, under whose dimensions the material properties of the materials were determined. The total failure probability S for a beam results from the sum of the factor R_i in each beam section over the entire beam length.

$$S = 1 - e^{-\mathrm{R_{total}}} \tag{3.13}$$

$$R_{\mathrm{total}} = \sum_{\mathrm{i}} R_{\mathrm{i}} \tag{3.14}$$

$$R_{\mathrm{i}} = \frac{L_{\mathrm{i}}}{L_0}\left(\frac{E}{\sigma_0}\right)^{\mathrm{m}} \frac{\varepsilon_{\mathrm{t,0}}^{\mathrm{m+2}} - \langle \varepsilon_{\mathrm{t,0}} - h\kappa_{\mathrm{y}} \rangle^{\mathrm{m+2}} - \langle \varepsilon_{\mathrm{t,0}} - b\kappa_{\mathrm{z}} \rangle^{\mathrm{m+2}} + \langle \varepsilon_{\mathrm{t,0}} - h\kappa_{\mathrm{y}} - b\kappa_{\mathrm{z}} \rangle^{\mathrm{m+2}}}{b_0 h_0 \kappa_{\mathrm{y}} \kappa_{\mathrm{z}} (m+1)(m+2)} \tag{3.15}$$

with	m/σ_0	*Weibull* constants
	$L_0/b_0/h_0$	Reference cross-section dimensions
	$L_i = \frac{L}{i}$	Section length
	$L = \frac{L}{i}$	Beam length
	i	Number of beam sections

Equations (3.13) - (3.15) can be used to determine the maximum acting load considering the size effect. Therefore, the acting load should be increased until the desired failure probability S is reached. Since EN 14080:2013 [5] specifies the material properties of glulam as 5% quantile values, it is recommended to limit the failure probability to the same value. The maximum tensile strain $\varepsilon_{t,0}$ can be used to determine the maximum tensile strength in bending $f_{t,0,size}$, see Eq. (3.16).

$$f_{\mathrm{t,0,size}} = \varepsilon_{\mathrm{t,0}} \cdot E \tag{3.16}$$

3.5. Calculation Procedure

To determine the load-bearing capacity of rectangular timber beams, the equations of geometrically non-linear behaviour (3.1) – (3.2), materially non-linear behaviour (3.5) – (3.11) and size effect (3.13) – (3.16) must be solved. For simplification, a graphical calculation approach is chosen. According to *Hörsting* [7] and *Töpler & Kuhlmann* [12], the maximum load-bearing capacity results from the intersection of the cross-section resistance $M_{y,R} - M_{z,R}$ and the internal force curve T2O $M_{y,II} - M_{z,II}$, see Figure 8. However, the load-bearing capacity might already be reached earlier, as material plasticising can lead to a decline of the load-deformation curve before the tensile strength in bending $f_{t,0}$ is reached (see Figure 8). Likewise, the maximum load-bearing capacity can be achieved after the intersection point if a higher tensile strength in bending $f_{t,0,size}$ applies at the lower beam edge due to size effect. It is important to note that an increase in the tensile strength in bending with an unchanged compressive strength $f_{c,0}$ increases the effect of plasticising and leads to a decrease in the load-bearing capacity curve according to size effect (see Figure 8). A more detailed description of the calculation method can be found in *Lukas* [8].

Figure 8 shows the load-bearing capacity curve for a rectangular cross-section with L x h x b = 6000 x 500 x 100 mm³, $E_{0,05}$ = 9600 N/mm², G_{05} = 540 N/mm², $f_{c,0}$ = f_m = 24 N/mm², e_y = L/1000, e_z = 0, e_ϑ = 1/100, using the structural system according to Figure 2 with a point load at midspan and varying axial forces. Until the elastic cross-section resistance $M_{y,el,R}$ – $M_{z,el,R}$ is reached, no plasticisation occurs in the cross-section and the load-bearing capacity curve follows the internal force curve T2O $M_{y,el,II}$ – $M_{z,el,II}$ in the first section (see Figure 8). At this point the tensile strength in bending $f_{t,0,el}$ results from the linear interaction of the stresses. The second section of the load-bearing capacity curve can be determined by varying the tensile strength in bending between $f_{t,0,el}$ and $f_{t,0,size}$. Within this section the cross section begins to plasticise. Figure 8 shows the elasto-plastic cross-section resistance $M_{y,el-pl,R}$ – $M_{z,el-pl,R}$ for a tensile strength in bending according to the bending strength $f_{t,0}$ = f_m. At the intersection of the elasto-plastic cross-section resistance $M_{y,el-pl,R}$ – $M_{z,el-pl,R}$ and internal force curve T2O $M_{y,el,II}$ – $M_{z,el,II}$ the cross-section stiffness can be updated with the help of the curvatures κ_y and κ_z to recalculated the internal force curve and determine a new intersection with the elasto-plastic cross-section resistance $M_{y,el-pl,R}$ – $M_{z,el-pl,R}$ [12]. This iterative process is repeated for all other tensile strengths in bending between $f_{t,0,el}$ and $f_{t,0,size}$ until the internal force curves T2O converge and the load-bearing capacity curve is obtained (see Figure 8).

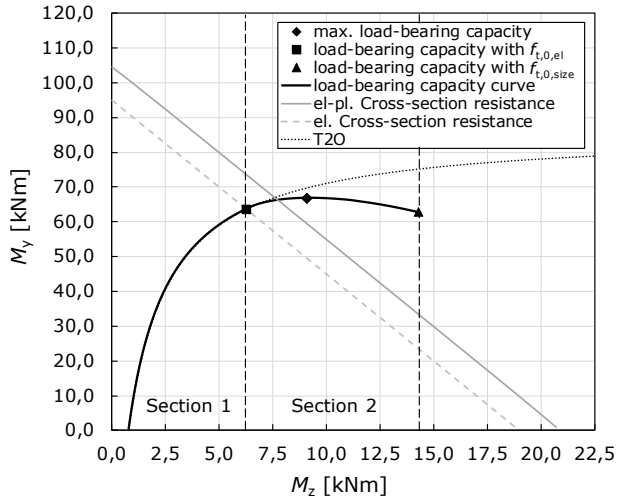

Figure 8: M_y-M_z-Interaction of a cross-section with h x b = 500 x 100 mm² made of GL 24h for N_x = -60 kN and point load at midspan.

4. Results

Figure 9 and Figure 10 show the load-bearing capacities $M_{y,R}$ of the experimental investigations by *Töpler & Kuhlmann* [13] for different slenderness $\lambda_{rel,m}$ and varying axial forces N_x. The load-bearing capacity $M_{y,R}$ decreases with increasing axial force N_x. The same pattern also results from the analytical model described in Section 3. The calculated curves in Figure 9 and Figure 10 are based on the experimental test program according to Table 1. For the material GL 24h, the material parameters $f_{m,mean}$ = $f_{t,0,mean}$ = 33 N/mm² and $f_{c,0,mean}$ = 40 N/mm² are assumed.

Table 1.: Test program for LTB on glulam GL 24h [13].

Beam number	Number of specimens	Span [mm]	Height x Width [mm²]	$\lambda_{m,rel}$*	N_x [kN]	$E_{0,mean}$ [N/mm²]	G_{mean} [N/mm²]
T01-T03	3	7880	720 x 120	1.04	0	12387	847
T04-T11	8	7880	600 x 120	0.94	0 to 75	12089	823
T12-T19	8	5880	480 x 120	0.74	0 to 105	11661	762

**With characteristic material values, taking into account an increase of $E_{0,05}$ × G_{05} by a factor of 1.4 according to DIN EN 1995-1-1/NA [4].*

Figure 9 shows the N_x-M_y curve with and without the size effect. Following the approach described in Section 3.4, the tensile strength in bending $f_{t,0,size}$ for the N_x-M_y curve with size effect exceeds the bending strength f_m. Since the bending strength f_m acts as the tensile strength in bending on the analytical model without size effect, the model with size effect reaches higher load-bearing capacities $M_{y,R}$. Due to the higher tensile strength in bending $f_{t,0,size}$, the plasticised area of the analytical model with size effect increases more. This leads to a lower increase in the load-bearing capacity caused by the size effect with rising axial force. When for the analytical model with and without size effect the same tensile strength in bending ($f_{t,0} = f_{t,0,size} = f_m$) is reached, the N_x-M_y curve coincides (see Figure 9 for $N_x \geq 180$ kN).
When compared, the N_x-M_y curves of the analytical model approximate the load-bearing capacities from the stocky test specimen well (see Figure 9). In particular, the N_x-M_y curve with size effect shows good agreement with the test results and illustrates the improvement of the load-bearing capacity by taking the size effect into account.

Since shear failure due to torsion is not considered in the analytical model according to Section 3 but frequently occurred for the slender test, the load-bearing capacity $M_{y,R}$ by the analytical model is overestimated for the slender test specimen by 10 to 20 % (see Figure 10).

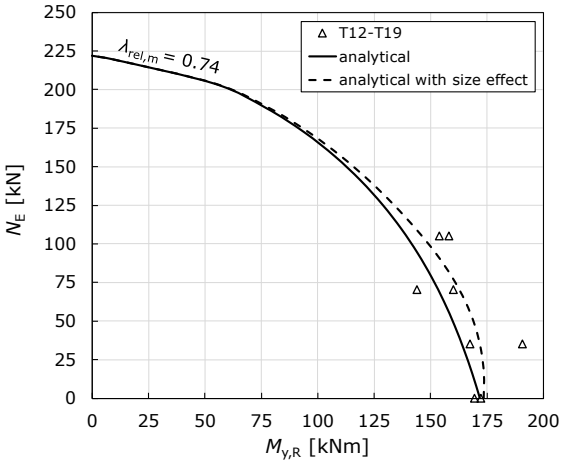

Figure 9: N_x-M_y-Curve of a cross-section with h x b = 480 x 120 mm² made of GL 24h with point load at midspan from analytical and experimental investigations T12-T19 [13].

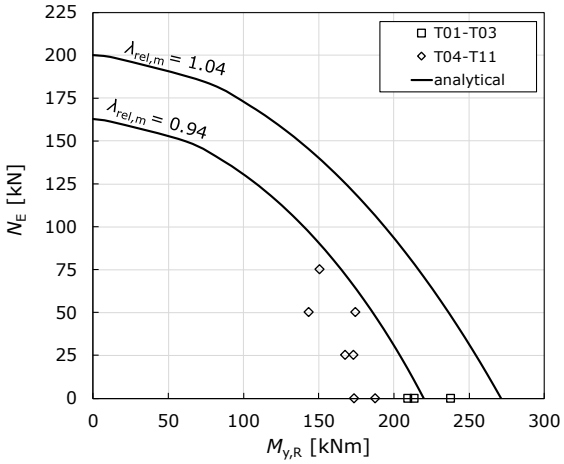

Figure 10: N_x-M_y-Curve of cross-sections with h x b = 600/720 x 120 mm² made of GL 24h with point load at midspan from analytical and experimental investigations T01-T11 [13].

5. Discussion

Figure 11 shows the N_x-M_y curves of the analytical model and T2O and ELM according to EN 1995-1-1:2004 [6]. These are calculated with the characteristic material values of GL 24h taking into account the increase of $E_{0,05} \times G_{0,05}$ by a factor of 1.4 according to DIN EN 1995-1-1/NA [4] and the cross-sectional dimensions according to Table 1 for the beam numbers T12-T19. According to prEN 1995-1-1:2023 [10], a bow imperfection of e_y = L/1000, a twist imperfection at midspan of $e_{\vartheta,mid}$ = L/(1500 x h) and a twist imperfection of the fork supports with high tolerances of $e_{\vartheta,supp}$ = 1/100 is assumed. Based on the investigations of *Töpler & Kuhlmann* [13], equivalent imperfections should be chosen for consistency in comparing different calculation methods. These are calculated to $e_{y,equi}$ = 5.88 mm and $e_{\vartheta,mid,equi}$ = 0.0091 m/mm.

The ELM according to EN 1995-1-1:2004 [6] follows a non-linear course, which results from the square of the bending component. For $\lambda_{rel,m}$ = 0.74 the reduction factor of k_m = 1.0 leads to a higher ultimate capacity $M_{y,R}$ for pure bending compared to the analytical model without size effect. With the introduction of the 2nd generation of Eurocode, the square in the bending component is omitted and a linear interaction is assumed. In addition, the imperfections $e_{y,equi}$ and $e_{\vartheta,mid,equi}$ are included in the determination of the reduction factors k_c and k_m [10]. As a result, the twist imperfection is also taken into

account. The same load-bearing capacities according to the analytical model without size effect are obtained for pure bending. The resulting N_x-M_y curve is linear and shows a difference in load-carrying capacity of up to 60% for combined bending and compression compared to the analytical model. Although the interaction of bending and axial force components according to EN 1995-1-1:2004 [6] cannot be justified mechanically, the N_x-M_y curve approaches the analytical model without size effect more closely so that differences of the load-bearing capacity are only up to 25%. Thus, the new regulations for the ELM significantly underestimate the load-bearing capacity of timber beams under combined bending and compression.

In order to still obtain a non-linear N_x-M_y curve in the 2nd generation of Eurocode, calculations can be carried out according to T2O. The equations described in Section 3.2 can be used for this purpose. In order to take the influence of the material non-linear behaviour into account, the axial force component in the design formula is squared [10]. The positive size effect on the bending strength can be considered by the k_{red} factor [10].

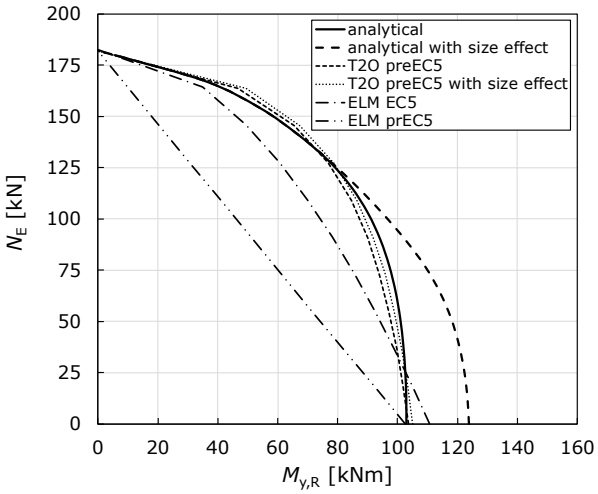

Figure 11: N_x-My curve of a cross-section with h x b = 480 x 120 mm² made of GL 24h with point load at midspan from analytical model, T2O and ELM at $\lambda_{rel,m}$ = 0,74.

Since prEN 1995-1-1:2023 [10] takes into account the three phenomena described in Section 3 in the design formula in a simplified way, the N_x-M_y curve according to T2O and the analytical models in Figure 11 are very similar. The positive effect of plasticising is thereby slightly underestimated by up to 3.5 % compared to the analytical approach from Section 3.3 [8], see Figure 11. Also, the load-bearing capacity of the analytical model increases up to 15 % when the size effect is taken into account. This size effect is caused by a favourable distribution of bending moments over the beam length, which is in agreement with the investigations of *Colling* [3]. Such effects cannot be considered with EN 1995-1-1:2004 [6] and prEN 1995-1-1:2023 [10]. Overall, the assumptions mentioned for T2O make its design much simpler than the design with the analytical model presented. However, it should be noted that no interaction of the three phenomena described in Sections 3.2 - 3.4 is considered with T2O. The reduction of the stiffness through plasticising and the associated influence on the geometrically non-linear behaviour, materially non-linear behaviour and the size effect can therefore only be assessed with an analytical model similar to the presented one. The implementation of the analytical model will be published within the framework of [14].

6. Conclusion and Outlook

An existing analytical model for the analysis of imperfection-sensitive timber beam-columns under combined N_x-M_y loading was further developed and is presented. The main components of the analytical model are described in Sections 3.2 - 3.4 and are based on the work of *Hörsting* [7] and *Töpler & Kuhlmann* [12]. As an extension, the deformation analysis of beams due to geometric and material non-linear behaviour is further developed. For this purpose, the beam is divided into an elastic and an elasto-plastic region along its length (Figure 7). Through numerical integration, the variable flexural stiffness

is taken into account in the deformation analysis. Additionally, the size effect is enhanced and a variable course of stresses over length, width and height of the beam is taken into account. Finally, the existing models assume that the maximum load-bearing capacity is reached when the internal forces exceed the cross-sectional resistance. However, the load-bearing capacity might already be reached earlier, as material plasticising can lead to a decline of the load-deformation curve before the bending strength is reached (see Figure 8). This can be considered now.

The analytical model shows good agreement with the experimental investigations of *Töpler & Kuhlmann* [13] (see Figure 9 and Figure 10). The ELM in 2nd generation of Eurocode leads to an underestimation of the load-bearing capacity $M_{y,R}$ for *N-M* interaction up to 60 %. A significantly higher load-bearing capacity can be determined with T2O according to prEN 1995-1-1:2023 [10]. Despite the simplification of the non-linear material behaviour, good agreement with the analytical model can be reached. Thus, T2O according to prEN 1995-1-1:2023 [10] represents the actual load-bearing capacity well. By taking the size effect into account with the model presented in Section 3.4, further increase in the load-bearing capacity of up to 15 % can be achieved.

Up to now, the analytical model only considers longitudinal stresses. However, the investigations by *Töpler & Kuhlmann* [13] show that shear failure can become decisive for loading situations with high shear stresses, such as three-point bending. The reason is additional torsional moments. An extension of the analytical model to include shear stress is therefore pending. In combination with experimental and numerical investigations, the analytical model can be used to derive optimised interaction formulas for the ELM. This would enable more economic results for *N-M* interaction.

7. References

[1] Abeysekera, I.; Feltham, I.; Lawrence, A.: *Buckling of slender timber beam-columns under combined loading, including creep*. In: 8th meeting of the International Network on timber Engineering Research (INTER), 54-2-1, Online meeting, 2021.

[2] Burger, N.: *Einfluss der Holzabmessung auf die Festigkeit von Schnittholz unter Zugbeanspruchung in Faserrichtung*. Dissertation, Ludwig Maximilian University Munich, Munich, Germany 1998.

[3] Colling, F.: *Einfluß des Volumens und der Spannungsverteilung auf die Festigkeit eines Rechteckträgers – Bestimmung der Völligkeitsbeiwerte, Anwendungsbeispiele*. In: Holz als Roh- und Werkstoff 44, S. 179-183, Springer Verlag, 1986.

[4] DIN EN 1995-1-1/NA: *Nationaler Anhang – National festgelegter Parameter - Eurocode 5: Bemessung und Konstruktion von Holzbauten – Teil 1-1: Allgemeines – Allgemeine Regeln und Regeln für den Hochbau*. German Institute of Standardization (DIN), Berlin, Germany, 2013.

[5] EN 14080: *Timber structures – Glued laminated timber and glued solid timber – Requirements*. European Committee for Standardization (CEN), Brussels, Belgium, 2013.

[6] EN 1995-1-1: *Eurocode 5: Design of timber structures – Part 1-1: General – Common rules and rules for buildings*. European Committee for Standardization (CEN), Brussels, Belgium, with corrections and amendments + AC:2006 and A1:2008, 2010-12.

[7] Hörsting, O.-P.: *Zum Tragverhalten druck- und biegebeanspruchter Holzbauteile.* Dissertation, Institut für Baukonstruktion und Holzbau, Technical University Braunschweig, Braunschweig, Germany, 2008.

[8] Lukas, J.: *Untersuchung der Momenten-Normalkraft-Interaktion biegedrillknickgefährdeter Holzträger*. Master thesis, Institute of Structural Design, University of Stuttgart, Stuttgart, Germany, 2023.

[9] Petersen, C.: *Statik und Stabilität der Baukonstruktionen. Elasto- und plasto-statische Berechnungsverfahren druckbeanspruchter Tragwerke: Nachweisformen gegen Knicken, Kippen, Beulen*. Friedr. Vieweg & Sohn, Braunschweig, Germany 1982.

[10] prEN 1995-1-1: *Eurocode 5 – Design of timber structures – Part 1-1: General rules and rules for buildings*. CEN/TC 250/SC 5 N 1729. European Committee for Standardization (CEN), Brussels, Belgium, 2023.

[11] Tapia, C.; Aicher, S.: *Size effect of glulam made of oak wood under consideration of the finite weakest link theory*. In: Proceedings of the 9th meeting of International Network on Timber Engineering Research (INTER), 55-12-2, Bad Aibling, Germany, 2022.

[12] Töpler, J.; Kuhlmann, U.: *Analytical and numerical investigations on imperfection-sensitive timber members subjected to combined bending and axial compression*. WCTE, Online meeting, 2021.

[13] Töpler, J.; Kuhlmann, U.: *Lateral torsional buckling of glulam beams*. In: Proceedings of the 10th meeting of International Network on Timber Engineering Research (INTER), 56-12-6, Biel/Bienne, Switzerland, 2023.

[14] Töpler, J.: *Load-bearing capacity of imperfection-sensitive timber members under combined bending and compression*. Unpublished, Dissertation, Institute of Structural Design, University of Stuttgart, Stuttgart, Germany, 2024.

[15] Weibull, W.: *A statistical theory of the strength of materials*. Generalstabens litografiska anstals förlag, Stockholm, Sweden, 1939.

Influence of adhesive joint thickness on the bonding quality of cross laminated timber

Paul Selmer
Regensburg University of Applied Sciences
Regensburg, Germany

Influence of adhesive joint thickness on the bonding quality of cross laminated timber

1. Starting point and research question

1.1. Quality of the adhesive bond

It is a complex process to produce solid wood panels from laminated timber according to standards. During the manufacturing process, there are three key factors that significantly contribute to the quality of the adhesive bond: the process itself, the adhesive used, and the raw materials. If any of these factors is not optimal, it can have negative effects on the quality of the bonding. In particular, the planing process and its results are crucial for the quality of the bond. Using improperly adjusted or heavily worn planer knives can lead to the planing of lamellae into a prismatic shape. Instead of a uniform cross-section, the end product has prism-shaped cross-sections, with one side thicker than the other. This results in unevenly thick adhesive joints.

But what impact does this have on the strength of the adhesive joint in the vacuum press process? Does an adhesive joint with an average thickness of 0.2 - 0.3 mm exhibit the same strength as an «optimal adhesive joint» with a thickness of 0.1 mm? This will be clarified in the experimental investigations of this study.

1.2. Quality assessment of the adhesive bond

The delamination test has proven to be a standard testing method for assessing the quality of adhesive bonding [1]. In general, the delamination test aims to subject bonded wood products to an artificial aging process. The respective test specimens are, therefore, soaked under precisely defined conditions with the influence of vacuum and pressure before being dried in the final step of the test method. This test simulates weather extremes that generate stress in the wood, resulting in cracks in the wood and the adhesive joints. The length and formation of these cracks provide an accurate assessment of the adhesive bond's quality.

In addition to the delamination test, the so-called rolling shear test is an essential part of quality control for laminated timber panels. The shear deformation in laminated timber components is quite complex due to the orthogonal arrangement of individual layers of boards and the resulting different shear moduli of these layers [2]. The shear modulus perpendicular to the fibers, known as the rolling shear modulus, is significantly lower than the shear modulus parallel to the fibers. Therefore, in a cross-section of laminated timber subjected to shear stress, rolling shear failure is typically the determining factor. This failure is characterized by a break tangential to the annual ring surfaces of the cross-layers [3].

A shear test is used to generate rolling shear, which is shear perpendicular to the fibers, in the middle layers. This test allows for testing the key strength properties of laminated timber components. However, testing the quality of adhesive joints is not possible with this test.

In the case of glued laminated timber, it is possible to assess the quality of the bonding through the shear test according to DIN EN 14080. In this test, the adhesive joints between the lamellae of glued laminated timber are subjected to monotonic shear stress until the adhesive joint reaches the point of failure. Due to the load introduction parallel to the fibers, there is no rolling shear stress in glued laminated timber. The adhesive joint is stressed up to the limit of the load. The failure case is either shear failure in the wood component or adhesive joint failure. Shear failure in the wood component is indicated by the proportion of fiber fractures. If the adhesive joint is split, the proportion of fiber fractures must be visually determined and rounded to the nearest number divisible by 5 for evaluation. The proportion of fiber fractures is defined as the wood fiber fracture portion

of a fracture surface [4]. The guidelines for assessing adhesive joints in existing glued laminated timber structures [5] mention, among other things, that the determined shear strengths are to be evaluated based on the proportion of fiber fractures present.
For laminated timber components, there is currently no standardized test for assessing adhesive joint shear due to the issue of rolling shear failure. Therefore, the question arises as to whether it is possible to assess adhesive joint quality through shear tests.

2. Experimental setup

2.1. Measuring the adhesive bond strength

Initial test attempts have revealed that due to the similar colors of wood and adhesive, it is challenging to clearly identify the thin adhesive joints with approximately 0.1 mm thickness under the microscope. The solution to this problem lies in a phloroglucinol solution, which discolors the wood surfaces but does not affect the adhesive joint.
To achieve uniform geometries of the test specimens, they were calibrated in terms of height and width using a wide belt sander before measurement. This allowed for an increase in measurement accuracy and speed.

Figure 1: Appearance under the microscope

Under the microscope, the adhesive joint is now clearly distinguishable in color from the wood surface. The boundaries of the joint are clearly visible.

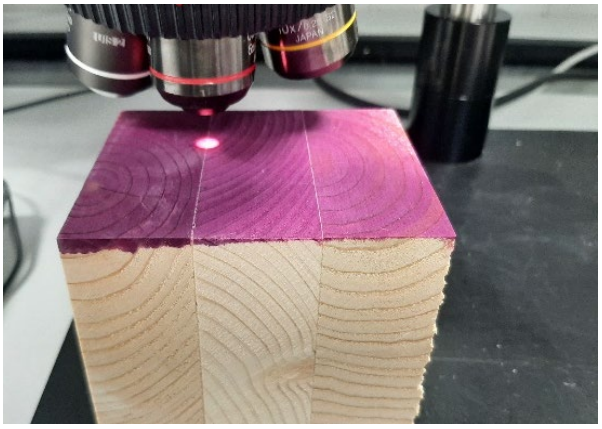

Figure 2: Test specimen sprayed with a solution

Spraying the test specimens with phloroglucinol solution causes the wood surface to turn violet, while the adhesive joint retains its original light color.

To investigate the effects of adhesive joint thickness on their load-bearing capacity, intentionally thicker adhesive joints need to be induced. Initial examinations under the microscope have revealed that the test specimens taken from the manufacturing process have adhesive joint thicknesses ranging from 0.1 mm to 0.15 mm, which is quite close to the «ideal» adhesive joint thickness of 0.1 mm.
To be able to analyze the load-bearing capacity of these joints, intentionally thicker joints need to be created first. Since there have been no comparable studies in this area, the development of a method for creating thicker adhesive joints is necessary as part of this work. In the preliminary experiments of this study, the joint thickness was modified by altering the planing geometry in the middle layers. Thicker joints in the range of 0.2 - 0.4 mm were achieved. The average joint thickness was determined by measuring two locations on two opposite sides of the test specimens.

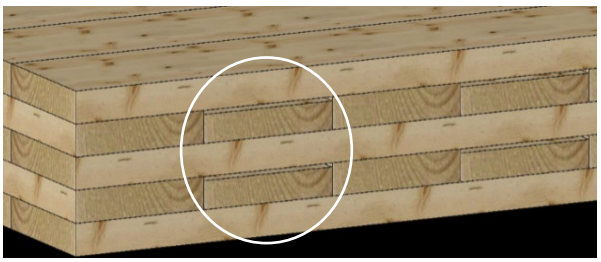

Figure 3: Production of CLT with modified joint thickness

By altering the planing thickness compared to the other lamellae, it should be possible to increase the joint thickness above the respective lamellae. In the above illustration, the offset between the layers is exaggerated for visual purposes. In reality, it is only 0.4 - 0.5 mm.

2.2. Shear tests & determination of fiber fracture proportion

After measuring the adhesive joints, shear tests will be conducted to determine their strength in shearing. The previously explained shear test for determining rolling shear strength is unsuitable for determining the shear strength of the adhesive joints. Since the rolling shear strength yields much lower values than the adhesive joint strength, this test primarily induces rolling shear failure. Therefore, the adhesive joint is not, or only to a limited extent, tested in this manner.
For glued laminated timber components, there is already a method for testing the shear strength of the adhesive joint through shearing. The significant difference compared to laminated timber panels lies in the force introduction parallel to the fibers. Rolling shear stress, as expected in laminated timber panels, does not occur in glued laminated timber due to its homogeneous fiber direction; the force is absorbed by the adhesive joint until it fails. When the adhesive joint is split, the proportion of fiber fractures must be visually determined for evaluation and rounded to the nearest number divisible by 5. The proportion of fiber fractures is defined as the wood fiber fracture portion of a fracture surface [4].

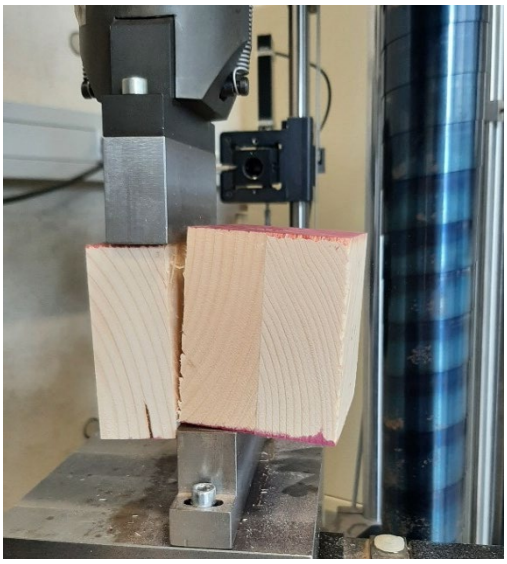

Figure 4: Shear test

The shear test is used to determine the shear strength of the individual test specimens in the area of the adhesive joint.

One possibility to primarily test the adhesive joint instead of the rolling shear failure of the wood in the shear test could involve rotating the test specimens by 45° relative to the fiber direction. This arrangement could potentially suppress rolling shear failure to some extent and only test the adhesive joint.

In the preliminary experiments, both 90° test specimens and test specimens rotated by 45° to the fiber direction were subjected to shearing. The evaluation revealed that the shear strength of the test specimens rotated by 45° was on average 50% higher, suggesting that at least part of the wood fracture in the form of rolling shear failure can be shifted toward adhesive failure. To accurately determine whether the failure of the adhesive joint is due to adhesive failure or wood failure, it is necessary to determine the proportion of fiber fractures at the fracture surface. The proportion of fiber fractures is visually determined with an accuracy of 10%.

The fracture patterns in the previously sheared preliminary test specimens differ noticeably. While the test specimens at 90° exhibit an average fiber fracture proportion of 67% and the predominant failure mechanism is attributed to rolling shear failure, the fiber fracture proportion in the test specimens at 45° is significantly lower, averaging 49%.

The results suggest that by rotating the test specimens at an angle of 45°, the adhesive joint is subjected to greater stress than in the standard test setup where the fiber direction of the top layer is parallel to the force direction. In the standard test specimens, as expected, rolling shear failure predominantly leads to shearing of the joint. In contrast, the test specimens at 45° exhibit a lower fiber fracture proportion, as suspected, indicating at least partial adhesive joint failure.

Figure 5: Fracture pattern at a 45° fiber angle

When the test specimen is cut from the component at a 45° angle to the fiber direction, rolling shear failure and, consequently, the proportion of fiber fractures are reduced.

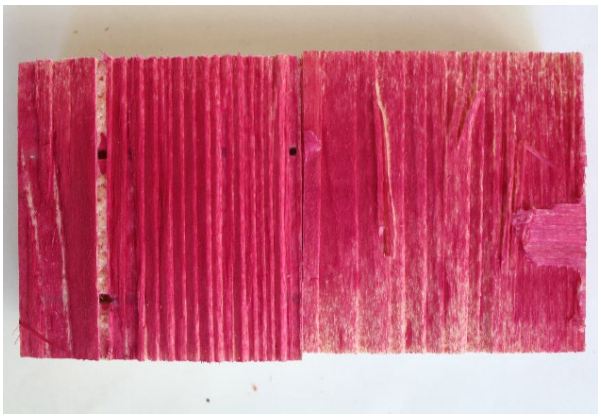

Figure 6: Fracture pattern at a 90° fiber angle

At a 90° angle to the fiber direction, rolling shear failure primarily determines the fracture pattern. The proportion of fiber fractures is accordingly high.

2.3. Test specimen fabrication

During the test specimen fabrication, a total of 4 different sample plate types are used:

Table 1: Adhesive application amount and expected joint thickness of individual sample plates

	Sample plate 1	Sample plate 2	Sample plate 3	Sample plate 4
Joint thickness	0,1 - 0,2 mm	0,1 - 0,15 mm	0,2 - 0,3 mm	0,3 - 0,4 mm
Application quantity	200 g/m²	150 g/m²	200 g/m²	400 g/m²

Sample plate 1 is intended to represent the typical production scenario. Using approximately 40 test specimens, an initial guideline for the average joint thickness should be established before determining an initial guideline for the adhesive joint's strength under normal conditions through shear tests.

Considering resource efficiency, sustainability, and cost-effectiveness, the question arises regarding the maximum required adhesive quantity. This will be reduced to 150 g/m² in sample plate 2. According to current knowledge, it is assumed that this reduction in adhesive quantity should result in slightly thinner adhesive joints. The subsequent shear tests will reveal the extent to which the reduced adhesive application affects the shear strength of the adhesive joint.

In sample plate 3, the «worst case» scenario in laminated timber production is simulated. The joint thickness is to be increased by approximately 200% while keeping the adhesive application quantity constant. The impact of this on the adhesive joint's strength and fracture pattern will be determined through shear tests.

Sample plate 4 aims to investigate whether a higher adhesive application quantity can counteract thicker joints.

3. Results

3.1. Joint measurements

The results of the joint measurements are presented in the following figure:

Sample plates 1 and 2, as well as 3 and 4, are geometrically nearly identical, apart from minor irregularities in planing. The different results of the average joint thickness values suggest that the adhesive application quantity contributes significantly to the strength of the adhesive joint. The results also indicate that it is indeed possible to modify the joint thickness to some extent through the modified planing of the middle layers.

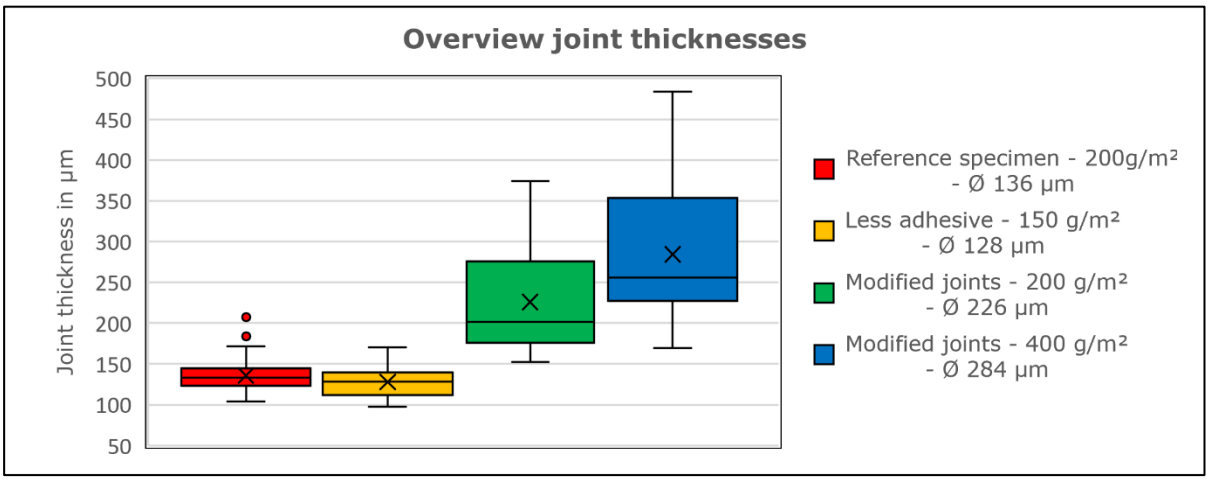

Figure 7: Overview of the distribution of joint thicknesses

The average values and standard deviations of the joint thicknesses for test specimen types 1 and 2 differ only minimally, while the average joint thicknesses and standard deviations for the intentionally modified joints of types 3 and 4 are significantly larger.

3.2. Shear tests

The results of the shear tests are presented in the following figure:

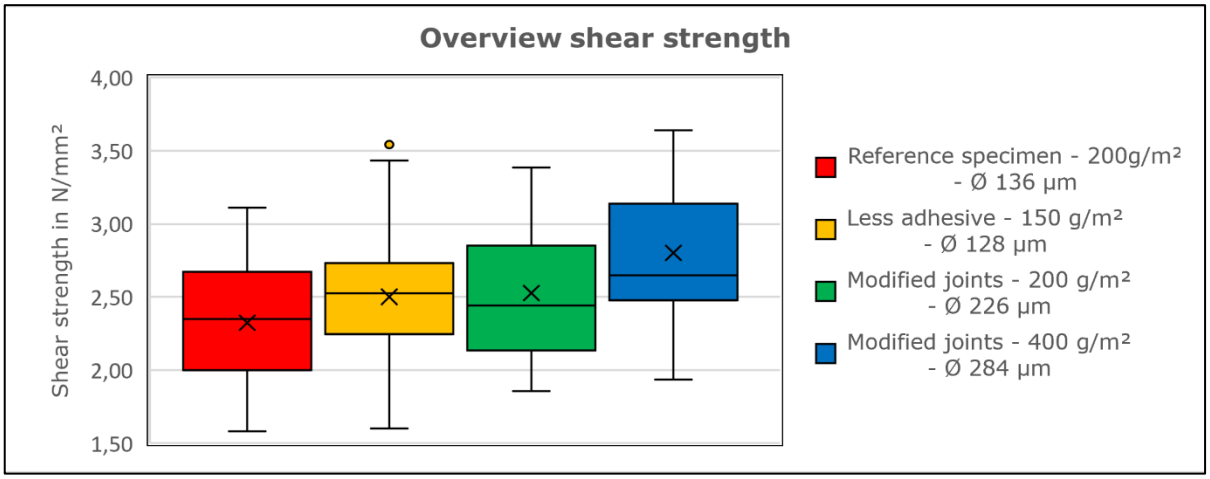

Figure 8: Overview of mean values and standard deviations of shear strength

The average shear strength of test specimen type 4 (double adhesive application quantity - 400 g/m² and modified joint thickness) is approximately 2.8 N/mm², almost 0.5 N/mm² higher than that of the reference test specimens (200 g/m²) with an average of 2.32 N/mm². The standard deviation for all 4 types falls within the range of 0.4 - 0.45 N/mm².

The evaluation of the different shear strengths yields a surprising result. While the adhesive joints of the reference test specimens have the «worst» performance with an average value of 2.32 N/mm², the average tensile strength with a lower adhesive application of 150 g/m² instead of 200 g/m² is almost 0.2 N/mm² higher. Also, the average shear

strength of the intentionally modified thicker joints through targeted planing in test specimen type 3 is higher than that of the reference plate. The significantly highest shear stresses were achieved in test specimen type 4 (modified joint thickness and double adhesive application quantity) with an average of 2.80 N/mm². Similar to the joint thicknesses, the values here also vary, with different degrees of deviation from the mean.

3.3. Determination of the fiber fracture proportion

The results of the determination of the fiber fracture proportion are presented in the following figure:

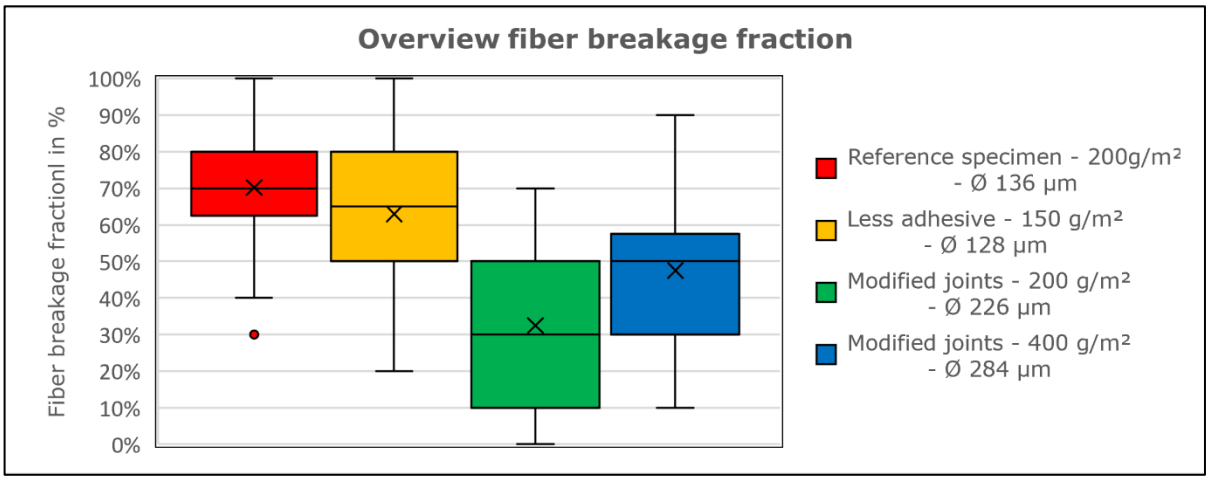

Figure 9: Overview of mean values and standard deviations of the fiber fracture proportion

The fiber fracture proportion is the highest in the reference plate, averaging 70%. For the test specimens of Sample Plate 2 (150 g/m²), the mean value is slightly lower at 63%. The lowest fiber fracture proportion and thus the highest adhesive failure proportion is observed in test specimen type 3 (modified joint thickness, 200 g/m²) with an average of 33%. Even with double the adhesive application quantity, the mean fiber fracture proportion is clearly higher at 48% compared to test specimen type 3, despite having thicker joints. The standard deviations of the fiber fracture proportions range from 17% to 22%.

The term «fiber breakage fraction» is synonymous with the term «wood failure.» The higher the fiber breakage fraction, the lower the proportion of adhesive failure. Conversely, a lower fiber breakage fraction indicates that the failure mainly occurred due to adhesive failure.

The test specimens of the reference plate are associated with the highest average fiber breakage fraction, approximately 70%. This means that in these test specimens, wood failure occurred in about 70% of cases and adhesive failure only accounted for 30%. There is a slightly lower fiber breakage fraction of approximately 63% in the test specimens of Plate 2, where the adhesive application amount was reduced to 150 g/m².

A clear difference in terms of the average fiber breakage fraction can be observed in the test specimens with modified joint thickness. In test specimen type 3 (adhesive application amount 200 g/m²), the average fiber breakage fraction is only 33%, and in test specimen type 4 (adhesive application amount 400 g/m²), it is 48%. Consequently, increasing the adhesive application amount results in a higher fiber breakage fraction, even with larger joint thickness, and, as a result, a lower proportion of adhesive failure.

4. Discussion of the results

In the evaluation of the experiments, it was observed that the fiber breakage fraction decreases noticeably in stronger joints. This implies, conversely, that in thicker joints, there is an expectation of a higher proportion of adhesive failure on average, with a decrease in the proportion of shear failure. Considering only the relationship between these two constants, it can be concluded that the bonding quality decreases with increasing joint thickness, as evidenced by the higher proportion of adhesive failure.

When you introduce the parameter of shear strength, the results seem contradictory at first glance: the greater the average joint thickness, the higher the average shear strength. However, when taking into account the fiber breakage fraction, the results make sense once again. The higher shear forces in thicker joints primarily result from adhesive failure and only to a minor extent from shear failure.

Therefore, there is a shift in the failure mechanism from the wood component to the adhesive joint. In the test specimens of the reference plate, the average fiber breakage fraction is relatively high at 70%. Before the adhesive joint fails here, the wood shears due to roll shear, as the roll shear strength is still lower than the adhesive joint strength despite the rotation of the test specimens by 45°. In the test specimens with modified joint thickness, this effect is exactly the opposite. Before wood failure due to roll shear occurs, the adhesive joint breaks.

According to these considerations, the quality of thicker adhesive joints is worse than that of components bonded under normal conditions, despite the seemingly higher shear strength. In comparing the test specimens of Type 3 (modified joints and adhesive application of 200 g/m²) with the test specimens of Type 4 (modified joints and adhesive application of 400 g/m²), it is noticeable that increasing the adhesive application not only increases the shear strength of the joint but also the proportion of wood breakage. Therefore, the quality of bonding appears to be better in Type 4 test specimens (modified joints & double adhesive application amount) despite the significantly greater joint thickness compared to Type 3 test specimens (modified joints).

Hence, in the case of thicker joints, the deteriorating quality of bonding can be improved by increasing the adhesive application amount.

5. Acknowledgements

I would like to express my thanks to my supervisor, Prof. Florian Scharmacher from OTH Regensburg, as well as Hirtreiter Holzbau GmbH and Jowat SE for their excellent support in the completion of this work.

6. Literature references

[1] Pöschl, Delaminierungsprüfung von Brettsperrholz. Vienna, 2018. available online at: https://www.holzkurier.com/holzprodukte/2018/11/delaminierungspruefung-von-brettsperrholz.html, accessed on [23.04.2023].

[2] Mestek, P.: Punktgestützte Flächentragwerke aus Brettsperrholz (BSP) - Schubbemessung unter Berücksichtigung von Schubverstärkungen. Dissertation, Technical University of Munich, Faculty of Civil, Geo, and Environmental Engineering, Munich, 2011.

[3] Wallner-Novak, M.; Koppelhuber, J.; Pock, Kurt.: Brettsperrholz Bemessung. Grundlagen für Statik und Konstruktion nach Eurocode. proHolz Austria, Vienna, 2013.

[4] Künniger, T.: Automatische Bestimmung des prozentualen Faserbruchanteils bei der industriellen Klebfestigkeitsprüfung. Final Report. Federal Materials Testing and Research Institute, Dübendorf, 2007.

[5] Dietsch, P.: Hochreiner, G.; Müller, A.; Scharmacher, F.; Wiegand, T.; Schulte-Wrede, M.: Merkblatt zur Bewertung von Klebfugen in Brettschichtholzbauteilen im Bestand. Studiengemeinschaft Holzleimbau e.V. (editor.), Wuppertal, 2021.

Concept Study on a Maximally Sustainable, Industrially Manufactured House with Wood Panel Construction

Pia Link
Rosenheim Technical University of Applied Sciences
Freising, Germany

Concept Study on a Maximally Sustainable, Industrially Manufactured House with Wood Panel Construction

1. Introduction and Background

Sustainability is a widely recognized concept, but its practical implications for the building industry remain unclear. Can demolition material be repurposed, and if so, how? What steps need to be taken to achieve the goals of the Paris Agreement, which seeks to limit global temperature increases to under 2°C (with a best-case scenario of 1.5°C)?
The construction sector is responsible for approximately 40 % of worldwide CO_2 emissions [1,2]. In Germany, buildings are responsible for 40 % of energy usage and 33 % of energy-related CO_2 emissions, due to their construction, operation, conversion, and dismantling [3]. Approximately 45 hectares of land are converted daily in Germany for transport and settlement areas [2].

2. Sustainability in the wood construction industry

Buildings are constructed with the intention of withstanding the test of time, thus demanding meticulous preparation pertaining to materials, practices, utilisation and lifespan maintenance. It is imperative to alter one's perspective, as buildings must be perceived as carbon sinks and dealt with accordingly [2].

2.1. Definition of Sustainability

The term 'sustainability' in Germany was coined by Hans Carl von Carlowitz, a chief miner in Saxony in the 18th century. In his book «Sylvicultura oeconomica», he emphasised the significance and imperative need for continuously sustainable use of the German forest for mining operations [4]. The modern interpretation of sustainability is based on the Brundtland report «Our Common Future», which was published in 1987 as part of the World Commission on Environment and Development (WCED) [5]. Sustainability is commonly depicted as a triangle or temple with three pillars representing environment, social, and economic aspects, highlighting the significance of a balanced and holistic system (Figure 1).

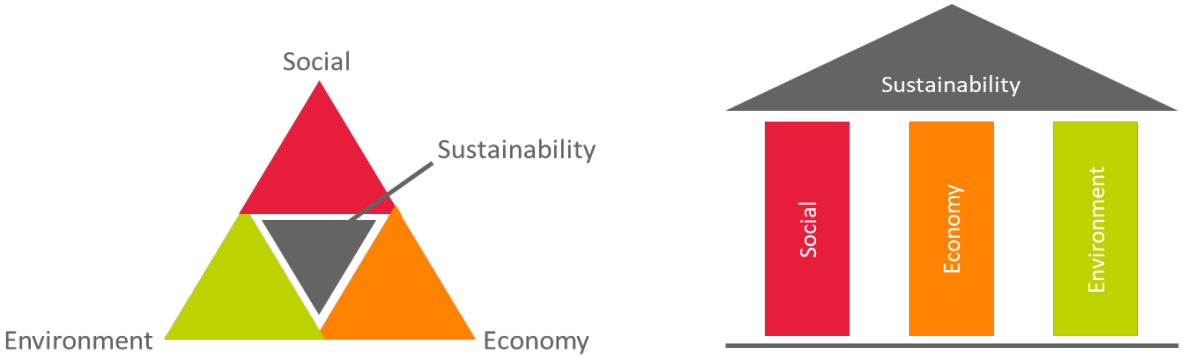

Figure 1: 3 Dimensions of sustainability (own illustration based on [1])

2.2. Wood Construction Industry

Forests cover approximately 31 % of the earth's land, which amounts to 4 billion hectares. These forests are primarily located in Russia, Brazil, Canada, USA, and China [6]. Active carbon sinks can be created through forests as approximately 50 % of wood is carbon. Trees absorb CO_2 from the atmosphere and release oxygen back into the environment through photosynthesis. The carbon gets stored in the tree trunks and wood. Native woodlands are in a state of equilibrium when it comes to biomass production. On the other hand, the removal of timber from a commercially managed forest results in the depletion of carbon storage. This, in turn, allows for more carbon sequestration by newly planted trees (Figure 2) [7,2].

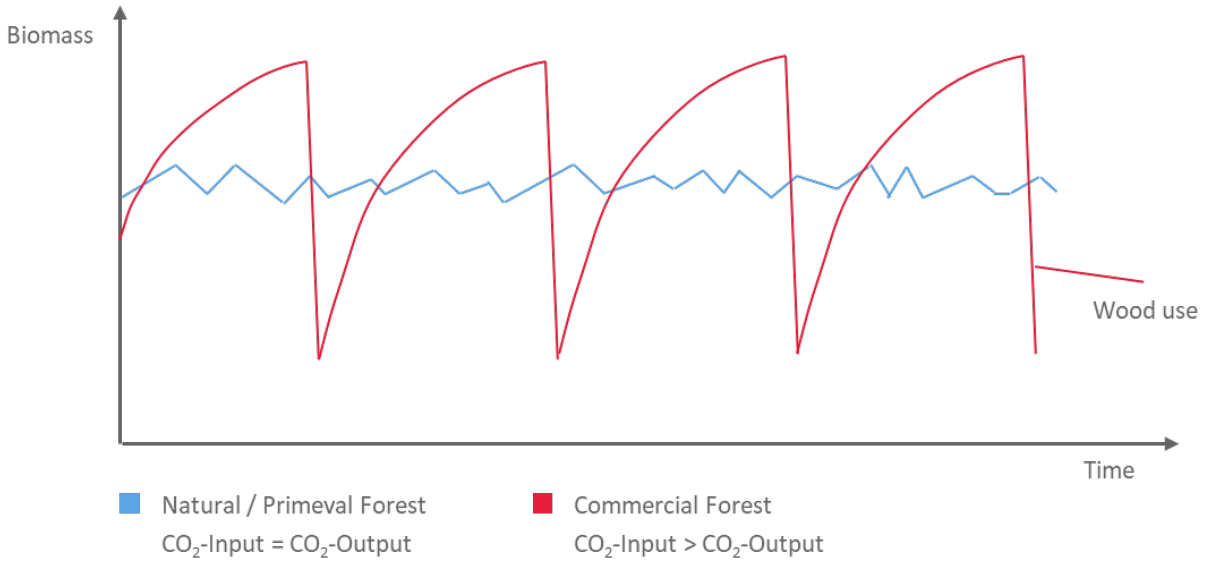

Figure 2: Comparison of biomass development for natural, primeval and commercial forest (own illustration based on [7])

One potential application for timber is in construction. Wood is a composite material consisting of cellulose fibres with large cavities. This allows timber to possess distinctive attributes such as high compressive and tensile strength, high load-bearing capacity, exceptional thermal insulation properties, and low weight compared to alternative materials. Timber can be employed as a replacement for concrete and steel or integrated into traditional building techniques.
The two principal wood construction systems are solid wood and wooden frame constructions. A significant advantage of timber construction is the ability to prefabricate individual components, including wall panels, elements, and complete room cells, within dry and constant workshop conditions. This ensures that assembly occurs before delivery to the construction site. Several process support mechanisms could be implemented, such as automated systems and ergonomic workstations for employees, resulting in high levels of quality and precision thanks to stable temperatures and organized workplaces [8–10].

2.3. Legislation in favour of sustainable development

To achieve the 17 Sustainable Development Goals ratified in Rio de Janeiro in 2012, governments worldwide are implementing legal guidelines and regulations for their citizens and businesses. These goals aspire to decrease poverty, enhance education and health to decrease inequality, advance economic growth while simultaneously combatting climate change and safeguarding oceans and forests [11]. Within the European Union, the Green Deal, EU-Taxonomy, and building resource passport / logbook were implemented to achieve the aim of net zero greenhouse gas emissions by 2050 [1,12,13]. The German government has been addressing sustainability for several years, but to comply with European standards, various regulations were enforced and updated. One recent development is the obligation to provide promotional loans and grants for construction by the Kreditanstalt für Wiederaufbau (KfW) [14], alongside the Building Energy Act [15].
For a loan to be granted, the building has to satisfy the «Qualitätssiegel Nachhaltiges Gebäude (QNG)» criteria. The QNG comprises five thematic quality fields – ecological, economical, social, technical, process and location quality – each encompassing an array of criteria amounting to 19 in total. The criteria are categorised into two parts – general and specific. Each of the 19 requirements must be met by at least one point. The certification offers two levels of achievement – PLUS or PREMIUM.
Since the certificate is a government label, three organisations in Germany are accredited to provide certification services at present (Figure 3) [16].

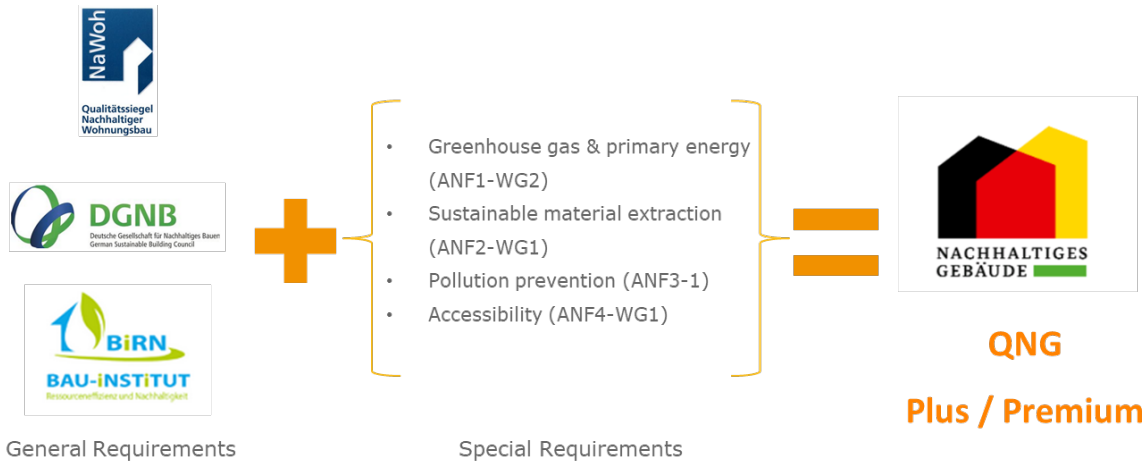

Figure 3: QNG Criteria

The certification process is overseen by a trained auditor appointed by each organization. The auditor consults with stakeholders and monitors the execution process. Optimal results are attained when the auditor is involved in the early planning phase, such as the design stage [17].
In contrast with global certifications (BREEAM and LEED), the QNG takes a holistic approach to sustainability with a 33% weighting assigned to each area (Figure 4).

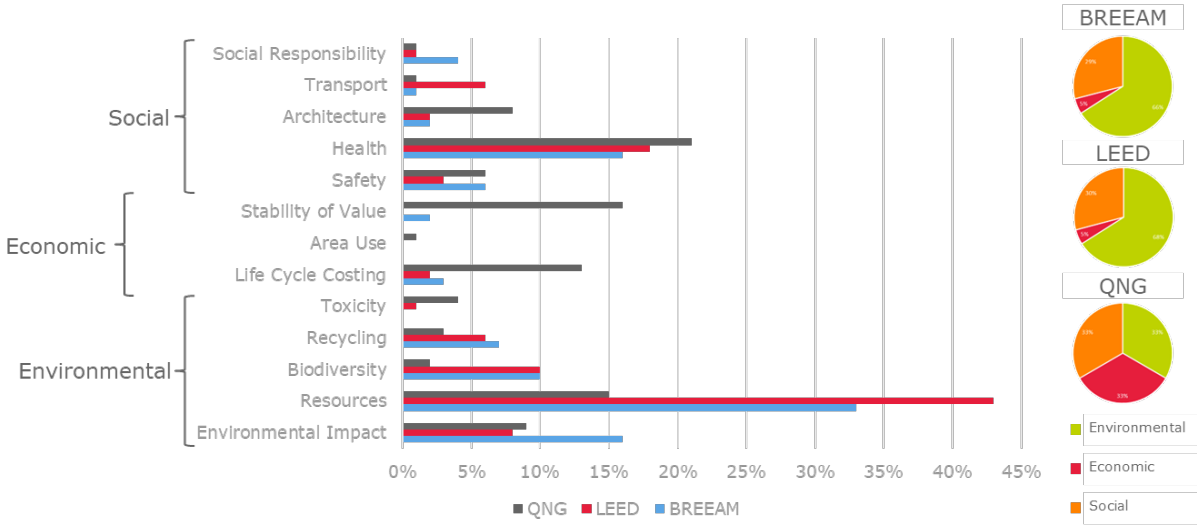

Figure 4: Comparison of international certificates BREEAM and LEED with QNG (own illustration based on [18])

3. Reuse, Recycle, Reduce – concepts and applications in construction

In 2020, Germany had access to approximately 8.3 million tonnes of waste wood. The majority, 60 %, was utilised for bioenergy purposes, with only 20 – 25 % being refurbished and reused. It is imperative that waste wood is perceived as a secondary resource as opposed to an energy source, and bioenergy should be considered only as a last resort [19,2].

3.1. Digitalisation

Digitalization is a ubiquitous term in all industries and aspects of daily life. Within the construction sector, particularly the wood construction industry, digitalization can have a significant effect and propel wooden structures to the forefront.
The loss of data when using disjointed software programs, lacking interfaces or reliance on pencil and paper, can lead to major deficiencies (Figure 5). One technology that can aid in the journey towards more sustainable buildings is Building Information Modelling (BIM). BIM assists in objective evaluation of building performance, and hence contributes

to achieving sustainability goals. The terminology will be elaborated upon in subsequent sections. This is a semantic data model that comprises physical and functional features, basically resembling a digital twin [1,20].

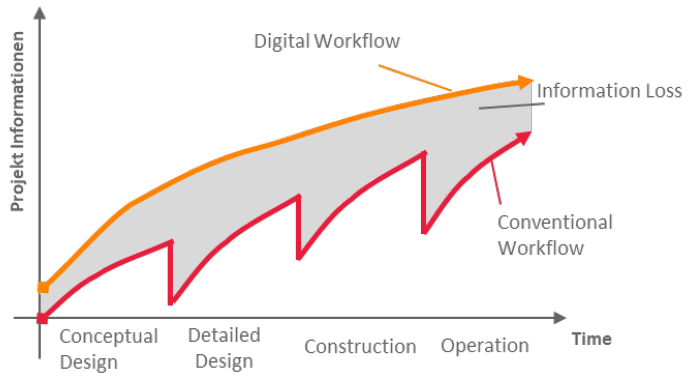

Figure 5: Comparison information flow conventional and digital workflows (own illustrations based on [20])

The most significant benefit can be achieved by utilising a BIG OPEN BIM at Level 3. This BIM database can be applied throughout the entire life cycle of a building, commencing from the conception stage up until the demolition. Interfaces are accessible for all relevant parties and data is automatically updated for individual use. The data model provides information on all materials and products used, maintenance, refurbishment, energy consumption during operation, and possible misuse. BIM can be employed to meet European regulations regarding the building resource passport / logbook. Additionally, data is accessible to support life cycle assessment and evaluate the building's value during its use and as a resource repository [1,20].

3.2. Life Cycle Assessment (LCA)

There are various potential applications for Life Cycle Assessment analysis, such as monitoring the supply chain management process or the procurement of materials and products. Within the construction industry, LCA is utilised for gathering and monitoring data on the environmental impact of materials and products. This encompasses their impact on global warming potential (GWP), CO_2 emissions, resource usage, particularly energy, and toxicity over the entire lifespan of the building. The methodical approach is defined by the DIN ISO 14.040 – 14.043 standard and is refined by various European norms.
There are three models available [21,22]:

- Cradle to Cradle
- Cradle to Grave
- Cradle to Gate.

For a comprehensive analysis, it is ideal to consider the entire lifespan of a building. The LCA result indicates that the use of wood and wooden products is notably superior to that of traditional construction materials. Timber grows naturally in forests, sequesters and stores C, and may serve as a heat source at the end of its life cycle, releasing the captured carbon. Unless the processes of transport and processing are taken into consideration, timber is considered to be entirely carbon-neutral.
Studies indicate that replacing mineral-based constructions with timber and wood-based materials in the construction of single and multifamily homes can reduce greenhouse gas emissions by up to 50 % [23].

3.3. Use of Materials

The digitalisation and monitoring of building life cycles are vital, as are the materials and products used in construction. These materials must possess durability and longevity whilst remaining innovative and renewable.
A vast range of renewable materials are available for thermal insulation, each with three important characteristics to consider [23]:

- Thermal conductivity λ
- Fire resistance
- Vapour diffusion resistance μ

In addition to wooden-based products, there are also annual crops such as hemp, straw, mycelium, and seaweed, as well as animal products like sheep wool and recycled materials such as plastic bottles.

3.4. Circular Economy

The present economic system is founded on a linear model whereby resources are extracted or gathered before undergoing a processing phase. The resulting goods are typically utilised just once and for a brief period before being disposed of. To achieve the 17 SDGs and limit the temperature rise to 2°C, the economic ethos must shift towards a circular economy (Figure 6).

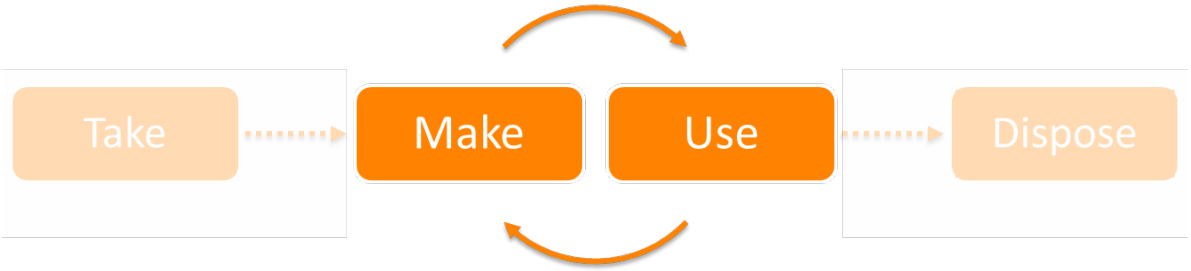

Figure 6: Circular Economy (own illustration based on [24])

In the circular model, there should be no waste as the end product of one usage phase becomes the starting point for another one. To achieve this, common practices include upcycling, downcycling, maintenance, and refurbishment. The Ellen MacArthur Foundation divides the circular model into two cycles, technical and biological. In the technical cycle, non-biodegradable materials and products are kept for as long as feasible. In the biological phase, biodegradable materials are deposited back into the environment for regeneration [24].
Wood and wood-based materials can follow a cascaded use, as shown in Figure 7. Many of these processes are already in place, but the quantity of them must be increased and the quality improved.

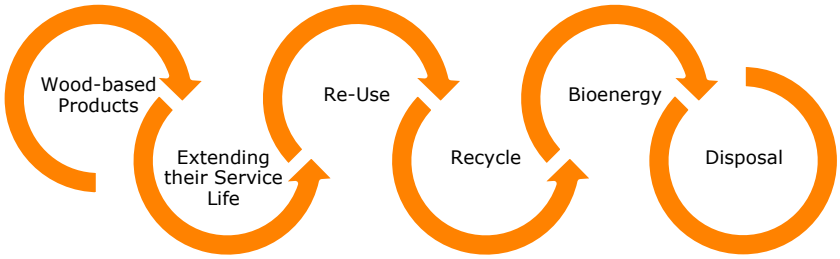

Figure 7: Cascading usage of wood and wood-based products (own illustration based on [25])

4. Comparison of different ecological insulation materials

For Table 1, D. Püschel and M. Teller edited ten different exterior wall constructions in preparation for a comprehensive life cycle assessment (LCA) analysis, based on the following pre-determined conditions: the assumed lifespan of the building is 50 years, all constructions display a uniform U-value of 0.2 W/(m^{2}K), and the LCA covers the production, use, repair, and end-of-life phases (LCA phases A – C, cradle-to-grave). A steel column construction was utilized as a supportive structure, integrated either within the wall structure of concrete and stone or in front of the wall for wooden constructions [26].

Table 1:Comparison of ten wall constructions (own illustrations based on [26])

			Wall Thickness in cm	Mass in kg/m²	PENRT in MJ/m²	GWP_{100} in kg CO_2 Eq./m²
Stone Wall	ST 1	Vertical perforated brick with perlite filling, lambda 0.07	52	431	871	71
	ST 2	Aerated concrete blocks, lambda 0.1 + thermal insulation plaster WLG 060	63	362	1051	127
	ST 3	Vertically perforated brick with rock wool filling, lambda 0.08	56	462	853	79
	ST 4	Three-layer aerated concrete, lambda 0.06	38	231	608	68
	ST 5	Sand-lime brick with ETICS	36	321	724	63
Reinforced Concrete Wall	StB 1	Reinforced concrete wall with mineral wool, back-ventilated and plastered	45	590	904	103
	StB 2	Reinforced concrete wall with ETICS and plastered	41	535	886	91
Wooden Panel Wall	HT 1	Wooden panel wall with mineral wool, back-ventilated and plastered	32+15	295	410	54
	HT 2	Wooden panel wall with rock wool and plastered	30+15	288	346	52
	HT 3	Wooden panel wall with cellulose fibre insulation and plastered	33+15	295	209	42

Compared with stone and concrete, wooden panel walls have superior advantages regarding wall thickness and mass, as well as lower primary energy demand non-renewable (PENRT) and GWP_{100} (Figure 8). In fact, ST 2 requires five times more energy than HT 3 and has a GWP that is three times higher than HT 3.

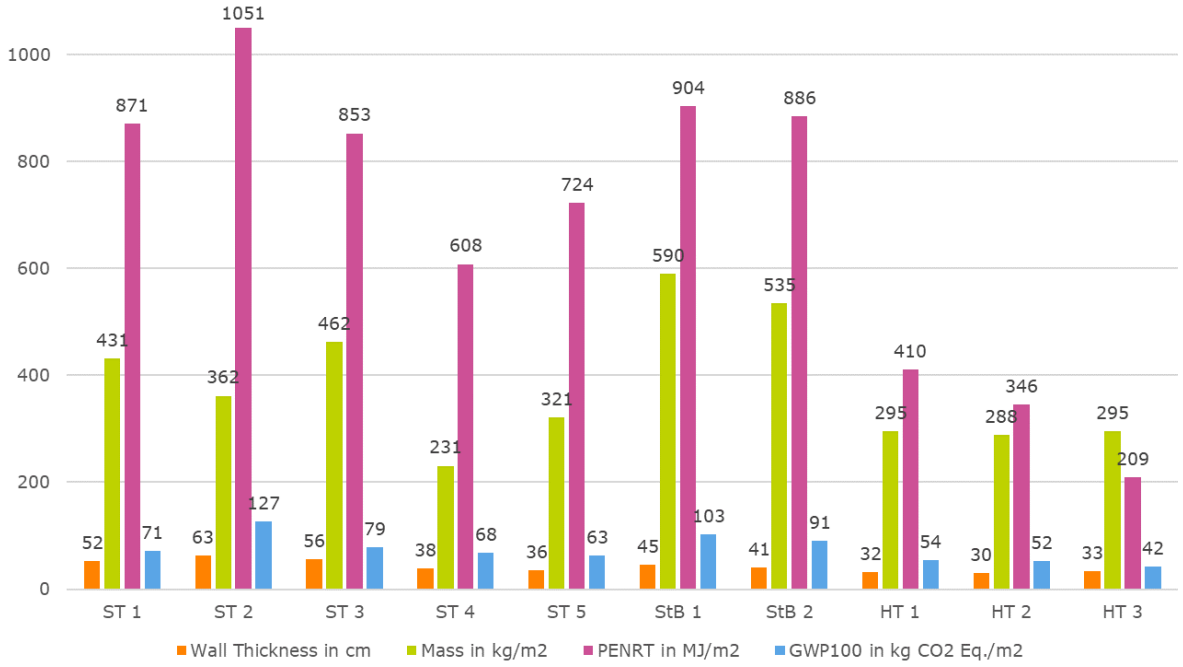

Figure 8: Wall construction evaluation (own illustration based on [26])

To elaborate, the wood panel construction «awrpi04a» was selected. Its overall structure and characteristics are detailed in Table 2 and visually presented in Figure 9.

Table 2: General wall construction «awrpi04a» (own illustration based on [27])

	Thickness [mm]	Building Material	Thermal Insulation λ	Thermal Insulation μ (min - max)	Thermal Insulation ρ	c	Fire Reaction Class EN
1	7	Plaster system	1,000	10 - 35	2000	1,130	A1
2	60	Wood-fibre insulation board WF-PT [045; 180]	0,045	5 - 7	180	2,100	E
3	160	Structural timber (60/..; e=625)	0,120	50	450	1,600	D
4	160	Variable insulation material					
5	15	OSB (airtight glued)	0,130	200	600	1,700	D
6	40	Spruce wood cross battens (a=400) or battens staggered	0,120	50	450	1,600	D
7	40	Variable insulation material					
8	12,5	Gypsum board type DF (GKF) or	0,250	10	800	1,050	A2
8	12,5	Gypsum fibreboard	0,320	21	1000	1,100	A2

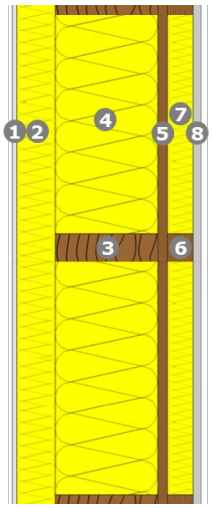

Figure 9: Graphical all construction (own illustration based on [27])

Four types of insulation materials were chosen for examination, as shown in Table 3. It is apparent that wood fire insulation and cellulose fibre walls have a lower U-value, indicating an improved performance compared to mineral wool.

Table 3: Insulation variants (own illustration based on [27])

Insulation Material	Thermal Insulation				Fire Reaction Class	U-Value Wall
	λ	μ (min - max)	ρ	c	EN	[W/(m²K)]
4 / 7 Mineral wool	0,040	1	16	1,030	A1	0,18
4 / 7 Sheep wool	0,041	1	30	1,720	E	0,19
4 / 7 Cellulose fibre	0,040	1	50	2,000	E	0,17
4 / 7 Wood fibre insulation	0,039	1 - 2	45	2,100	E	0,17

Table 4 presents a comparison of selected LCA indicators, with their corresponding visualisation in Figure 10.

Table 4: LCA of insulation variants (own illustration based on [27])

per m² construction surface	Unit	awrpi04a-11 Mineral wool	awrpi04a-10 Sheep wool	awrpi04a-09 Cellulose fibre	awrpi04a-14 Wood fibre insulation
GWP (A1 - A3)	kg CO_2 Eq.	-27,806	-26,098	-33,761	-35,984
AP (A1 - C4)	kg SO_2 Eq.	0,16	0,129	0,141	0,140
ODP (A1 - C4)	kg R11 Eq.	3,14E-06	2,97E-06	2,68E-06	2,87E-06
PERT (A1 - A3)	MJ	739,730	763,304	760,928	813,755
PENRT (A1 - A3)	MJ	596,561	545,234	507,759	573,731
Mass of renewable raw materials used	kg	36,895	38,153	41,522	41,324

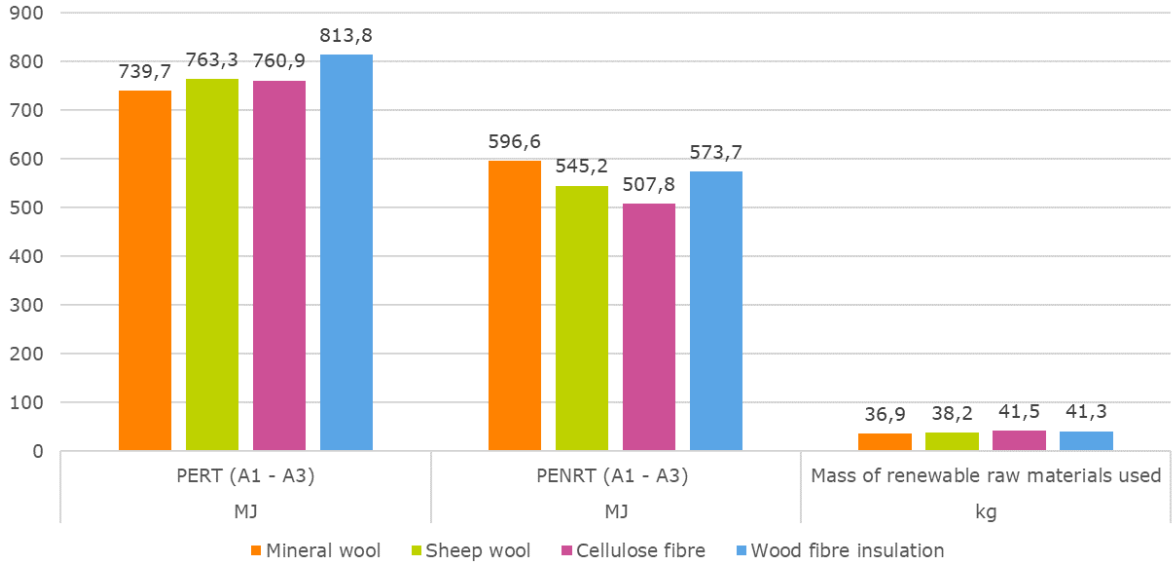

Figure 10: LCA of insulations variants (own illustration based on [27])

It is evident that renewable insulation materials outperform conventional materials in terms of primary energy demand renewable (PERT) and PERNT. Among all the renewable materials, wood fibre insulation demands the highest energy as the production process is rather energy intensive. Generally speaking, it should be noted that renewable (insulation) materials may cost more, but their social and ecological benefits are significant and cannot be overlooked. For this wall construction, it is advisable to opt for a renewable material due to its superior insulation qualities [27,26].

5. Conclusion

In conclusion, most of the solutions are currently available. It should be noted that several ecologically sound, healthy, and reasonably priced products and constructions have already been verified and authorised by numerous users, institutes, and governments.
One example is the building project at the former airfield Berlin-Tegel, Germany. The housing for around 10,000 people will be built 20 % more cost-effective than conventional massive construction [2]. However, it must be acknowledged that sustainability is not economical in the short term, and this presents a significant challenge. It is crucial that we communicate this message to our leaders and society. Our perspective towards the environment and natural resources must change. Every building should be regarded as a resource hub rather than a burden. Sustainability is a long-term objective, and we must remember that its benefits may not be realized by the present generation. Our goal is to improve and prosper over the long term, benefiting future generations.

6. Bibliography

[1] Bartels, N., Höper, J., Theißen, S., and Wimmer, R., *Anwendung der BIM-Methode im nachhaltigen Bauen. Status quo von Einsatzmöglichkeiten in der Praxis,* Springer Fachmedien Wiesbaden, Wiesbaden, 1 Jan. 2022.

[2] Wiegandt, K., *3 Grad mehr. Ein Blick in die drohende Heißzeit und wie uns die Natur helfen kann, sie zu verhindern,* Oekom Verlag, München, 1 Jan. 2022.

[3] Deutsche Gesellschaft Nachhaltiges Bauen e. V. (DGNB), «Heute für morgen bauen,» 1 Dec. 2018.

[4] Carlowitz, H. C. von, *Sylvicultura Oeconomica. Haußwirthliche Nachricht und Naturmäßige Anweisung zur Wilden Baum-Zucht,* Brauns Erben, Leipzig, 1 Jan. 1713.

[5] World Commission on Environment and Development (WCED), «Report of the World Commission on Environment and Development: Our Common Future: Brundtland-Report,» 1 Jan. 1987.

[6] Statista GmbH, «Waldfläche und Waldzustand weltweit,» URL: https://de.statista.com/themen/7066/waelder/#topicOverview [retrieved 1 May 2023].

[7] Herzog, T., Natterer, D.-I. J., Schweitzer, R., Volz, D.-I. M., and Winter, W., *Holzbau-Atlas,* 4th ed., Institut für internationale Architektur-Dokumentation GmbH & Co. KG, München, 1 Jan. 2003.

[8] Dangel, U., *Wendepunkt im Holzbau. Neue Wirtschaftsformen,* Birkäuser Verlag GmbH, Basel, 1 Jan. 2017.

[9] Huth, U., «Holz im Wandel der Erfordernisse für das Bauen,» *Bund Deutscher Zimmermeister im Zentralverband des Deutschen Baugewerbes e. V.*, 1 Jan. 2009.

[10] Kober, V., «Holztafelbau beim Fertighaus: Alle Infos, Vorteile & Nachteile,» URL: https://www.wohnnet.at/bauen/bauvorbereitung/holztafelbauweise-42292 [retrieved 6 February 2023].

[11] United Nations Department of Economic and Social Affairs, «THE 17 GOALS | Sustainable Development,» URL: https://sdgs.un.org/goals#history [retrieved 10 April 2023].

[12] European Commission (ed.), *Der europäische Grüne Deal,* Brüssel.

[13] Buildings Performance Institute Europe (BPIE), «Fahrplan zur Integration einer Lebenszyklusperspektive im Gebäudebereich in Deutschland,» 1 Jan. 2023.

[14] KfW Bank, «Wohngebäude – Kredit (261),» URL: https://www.kfw.de/inlandsfoerderung/Privatpersonen/Neubau/F%C3%B6rderprodukte/Bundesf%C3%B6rderung-f%C3%BCr-effiziente-Geb%C3%A4ude-Wohngeb%C3%A4ude-Kredit-(261-262)/ [retrieved 22 February 2023].

[15] Presse- und Informationsamt der Bundesregierung, «Gesetz zum Erneuerbaren Heizen: Für mehr klimafreundliche Heizungen,» URL: https://www.bundesregierung.de/breg-de/aktuelles/neues-gebaeudeenergiegesetz-2184942 [retrieved 1 October 2023].

[16] Bundesministerium für Wohnen, Stadtentwicklung und Bauwesen (BWSB), «Qualitätssiegel Nachhaltiges Gebäude (QNG) - Informationsportal Nachhaltiges Bauen,» URL: https://www.nachhaltigesbauen.de/austausch/beg/ [retrieved 27 April 2023].

[17] Bundesministerium für Wohnen, Stadtentwicklung und Bauwesen (BWSB), «QNG Handbuch,» 1 Mar. 2023.

[18] Jensen, K. G., and Birgisdottir, H., «Guide to Sustainable Building Certifications,» 1 Aug. 2018.

[19] Fachagentur Nachwachsende Rohstoffe e. V. (FNR), «Charta für Holz 2.0: Kennzahlenbericht 2021 Forst & Holz,» 1 May 2022.

[20] Borrmann, A., König, M., Koch, C., and Beetz, J. (eds.), *Building Information Modeling. Technology Foundations and Industry Practice,* Springer International Publishing, Berlin, Heidelberg, 1 Jan. 2018.

[21] Deutsches Institut für Normung e. V. (DIN), «Umweltmanagement – Ökobilanz – Grundsätze und Rahmenbedingungen,» No. 14040, 2006th ed., Beuth Verlag GmbH, Berlin, 1 Feb. 2021.

[22] Liebsch, T., «Ökobilanz (LCA) - Vollständiger Leitfaden für Einsteiger: Vollständiger Leitfaden für Einsteiger,» URL: https://ecochain.com/de/knowledge-base/oekobilanz-lca-kompletter-leitfaden-fur-anfanger/ [retrieved 24 June 2023].

[23] Kaufmann, H., Krötsch, S., and Winter, S., *Atlas mehrgeschossiger Holzbau. Grundlagen, Konstruktionen, Beispiele,* 4th ed., DETAIL Business Information GmbH, München, 1 Jan. 2022.

[24] Ellen MacArthur Foundation, «Cirular Economy,» URL: https://ellenmacarthurfoundation.org/ [retrieved 15 March 2023].

[25] European Union, «Nature Factsheet,» 1 Jul. 2021.

[26] Püschel, D., and Teller, M. (eds.), *Umweltgerechte Baustoffe. Graue Energie und Nachhaltigkeit von Gebäuden,* Fraunhofer IRB Verlag, Stuttgart, 1 Jan. 2013.

[27] Holzforschung Austria – Österreichische Gesellschaft für Holzforschung, «dataholz.eu,» URL: https://www.dataholz.eu/ueber-dataholzeu.htm [retrieved 12 May 2023].

Circularity in Timber Construction

Leoni Lichtblau
School of Engineering and Design
Technical University Munich
Munich, Germany

Circularity in Timber Construction

1. Introduction

Our buildings are among the most complex and long-lasting economic structures. The staggering levels of waste accumulation and the immense need for raw materials and energy in the construction industry make it evident that we need a paradigm shift in the building sector. The most pressing challenges of our time are resource scarcity, social challenges, and climate change. Several strategies are essential for a true transformation: a moratorium on demolitions, sustainable building techniques, and the establishment of a circular economy. Over recent centuries, significant economic and human resources have been invested in research and development, focusing on energy efficiency, renewable building materials, and economic optimization. Circular practices are relatively new at the forefront, but their significance is increasingly recognized. Where up until now existing structures are mostly cherished for an aesthetic value provided by e.g. details like oak beams or hand crafted tiles, a circular economy reimagines our human-made resource deposits as urban mines, where elements are considered and reused before extracting new resources. This approach avoids harmful interventions in nature and reduces energy-intensive, CO2-emitting manufacturing. The circular economy is a crucial driver of forward-looking and sustainable architecture, with its central strategies including sufficiency, reuse, recycling, repurposing, and even downcycling. It should replace the lowest levels, such as thermal utilization, landfills, and environmental pollution (like microplastics), which still belong to the linear economy.

For my master's thesis, I undertook the case of «Timber as the ideal building material for a circular construction technique». My initial goal was to acquire scientific knowledge to develop a prototype construction and design strategy based on this foundation. This strategy aimed to meet new functional requirements in a circular and sustainable way through increased flexibility.

2. Status Quo

Timber proves highly suitable for circular architecture due to its properties and potential. Sustainable forestry practices enable a continuous and healthy cycle. The value and significance of wood are on the rise, driven by the growing emphasis on sustainable forest management and the reuse of existing timber. However, current practices often hinder timber's full potential due to the way components are connected. Joints play a pivotal role in enabling subsequent use, necessitating mono-material and (or reversible connections. I compiled the results of my extensive research in literature, participation in congresses, and discussions with experts, researchers, professors and practitioners into a book.

2.1. Matured Timber

There are three primary avenues for utilizing matured timber: material use, energetic use, and biological composting. The classification of wood follows regulations set by various acts and ordinances. The key criterion in this classification is the degree of contamination by chemical impurities. [1] Presently, 90% of matured timber is primarily used for thermal applications, while only 10% is recycled in chipboard production. (cf. figure 1) This is largely due to challenges in separating materials caused by glue or lacquer and the limited profitability of recycling waste wood.

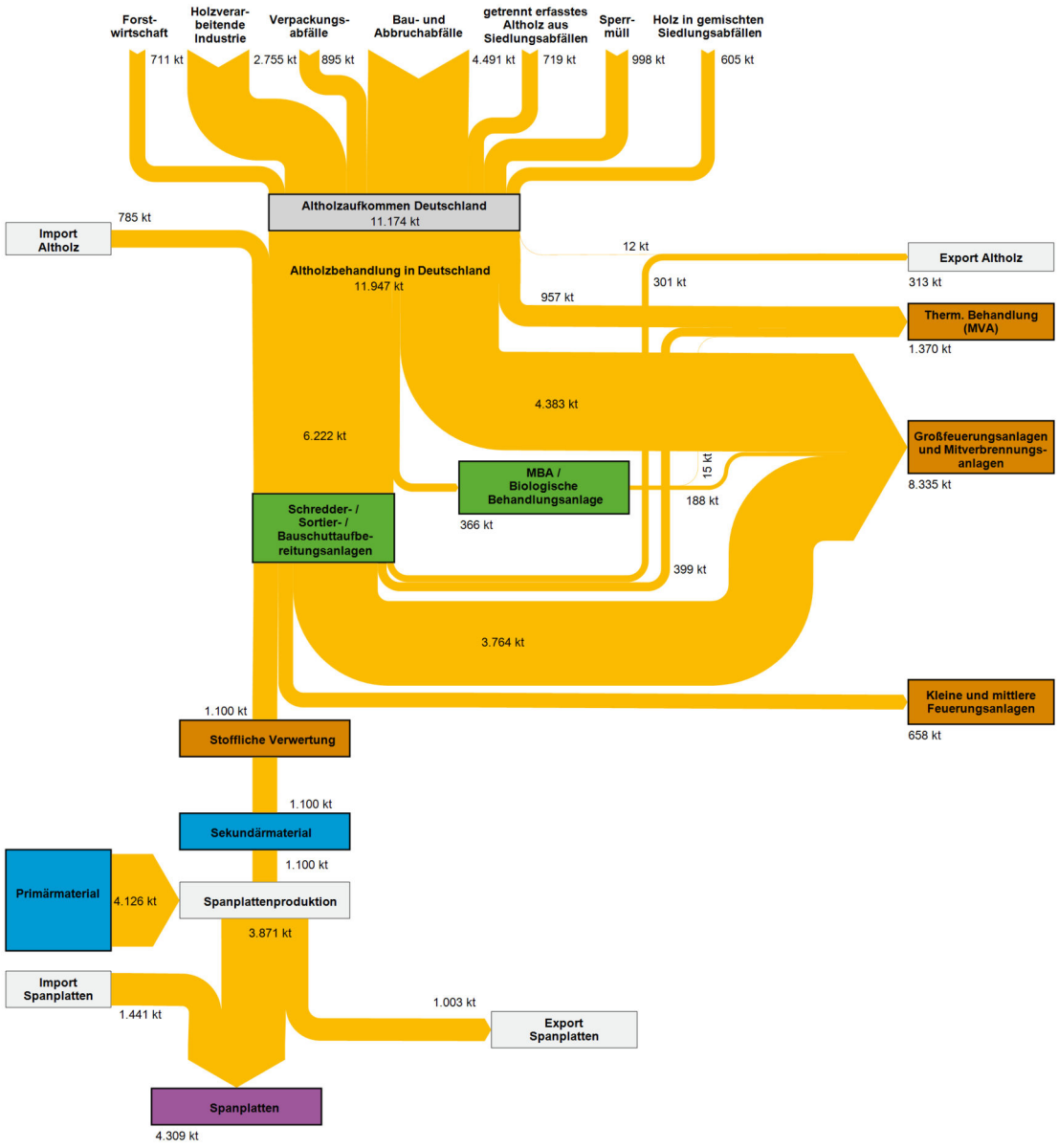

Figure 1: Material flows for waste wood recycling in Germany 2015

2.2. Cascade potential of timber

Timber benefits from its many native properties: the usage of cascades enables a multiple extension of the life cycle of a timber component, it maximizes the duration of carbon storage and allows a continuing substitution of carbon-emitting mineral and fossils resources. [2] Nevertheless, reuse comes first in terms of value creation or preservation potential and therefore a circulation of the timber component in the high cascades as long as possible. As a result, cascade use is a proven remedy against scarcity of raw materials as well as the independence of supply chains.

2.3. Drawbacks

At the moment large scale high value reuse as proposed is not yet feasible. [3] As already mentioned matured timber is often contaminated with chemical impurities and therefore only has low value. For a mono material separation a technical implementation is mostly still missing. In addition building elements are often damaged due to the dismantling process, the quality and the characteristics of the material and therefore a use at an equal cascade is mostly not possible.

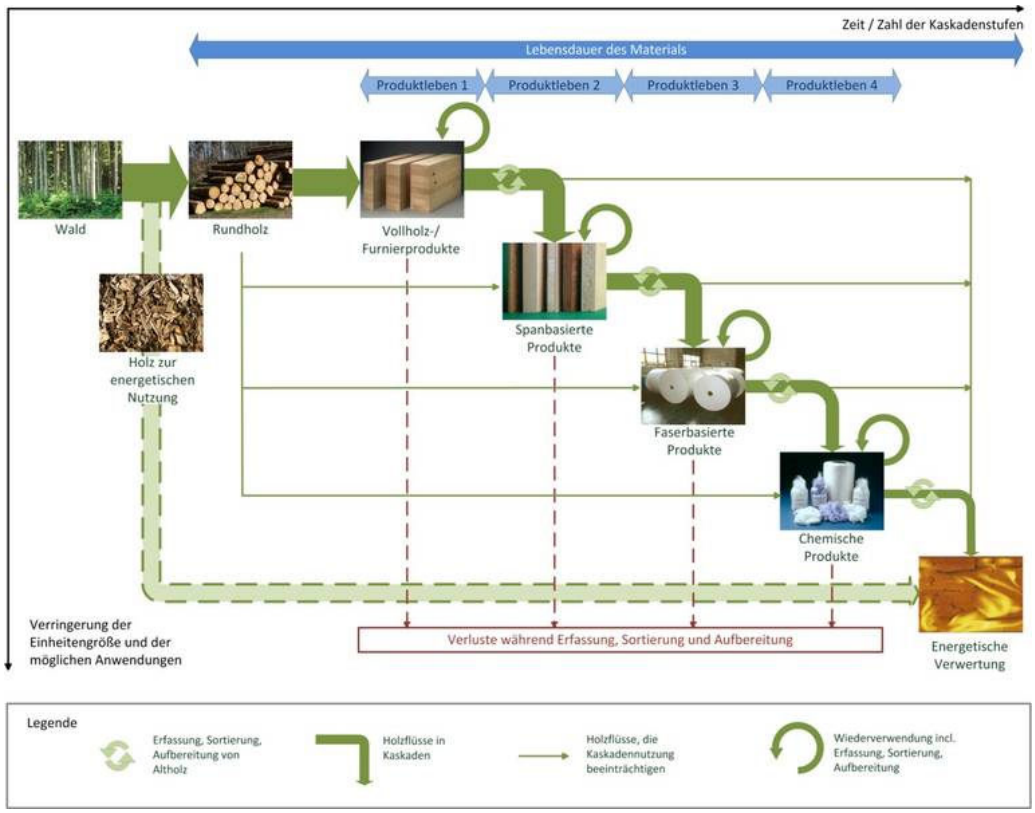

Figure 2: Cascade usage of timber, Höglmeier et al. 2016

2.4. Conclusions

Leveraging the cascades offers significant benefits in terms of resource efficiency and environmental impact reduction. A pivotal step involves transforming the building material market and replacing non-timber products with sustainable alternatives. While the total volume of matured timber is increasing, it varies in quality.

To establish a bio-based circular economy, the fundamental key lies in product design aligned with circular principles. This approach is crucial for a sustainable and eco-conscious future.

3. Knowledge of the past

3.1. Scarcity of timber

Throughout history, human innovation often emerges out of necessity. In Europe, the forest resources faced severe depletion due to industrialization and the growing human population. Demand for timber was soaring, while the availability was dwindling. Timber was also the primary energy source during this period. It wasn't until the mid-18th century that the timber supply improved with the discovery of coal as an alternative energy source. Before this turning point, people sought economic solutions to cope with the scarcity of timber through creative construction methods. [4]
The type of joints used in construction was profoundly influenced by this scarcity and played a pivotal role in architectural design.

One of the simplest ways to combine functional and economic aspects with building design was through timber-in-timber joints. For instance, in response to the scarcity of timber, innovative construction methods like the «Bogenbinder» emerged. This alternative roof construction efficiently used timber pieces by adding small components. [5]

Another notable development was the «Polonceau-Binder» which cleverly integrated timber with steel in areas where it was structurally efficient. According to Polonceau, the individual parts of this construction could be easily disassembled for transportation and were suitable for reuse. [6] The key was creating a material-appropriate combination of timber and steel, leveraging the unique properties of each material to form efficient and slim structures.

3.2. Japanese timber joints

The history of Japanese architecture provides a wealth of knowledge about timber constructions and elaborate joints. I delved deeply into Japanese timber architecture during my theoretical research. Many of their joints are reversible due to their fundamental principle of form-fitting plug-ins. These ancient carpentry techniques are still in use today and can be economically efficient with the help of modern CNC milling machines.

I spent several weeks studying the possibilities of Japanese timber joints and even developed a reversible joint based on original Japanese designs that could be suitable for mass production. However, I decided not to pursue this approach further due to the joint's complexity and the challenge of assessing its dismantling capabilities without practical testing. While it could have offered mono-material characteristics, it might not have been economically viable. Nevertheless, this exploration provided valuable insights that contributed to the final approach.

4. Development of a circular construction principle

4.1. Approach and requirements

I began my journey by reevaluating the endurance of various layers within a structure. This led to the formulation of fresh hypotheses regarding the lifespan of individual component layers. It is now of paramount importance to establish revised durability standards. To facilitate non-invasive repairs or replacements, it is crucial to create reversible connections between these layers, each having its own distinct service life. Primary objective was to achieve variability, longevity, and reversibility while adhering to circular principles, including resource-saving, simplicity in construction, and joint elements.

4.2. The structural principle

To attain high variability, a skeletal structure was chosen, albeit with acoustic limitations for residential purpose. Nevertheless Prof. Dr.-Ing. Jürgen Graf from the TU Kaiserslautern considers this construction to be the most suitable for circular construction and flexibility. To overcome this limitation, I integrated load-bearing timber frame panels, enabling acoustic separation and thus decouple the usage units. (cf. figure 3)

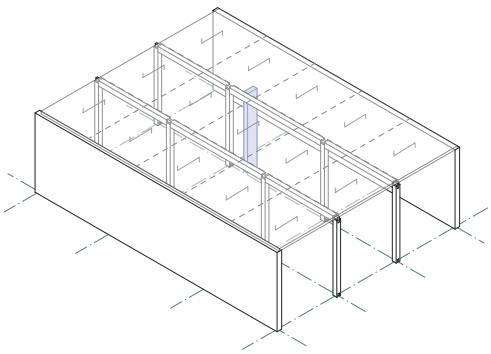

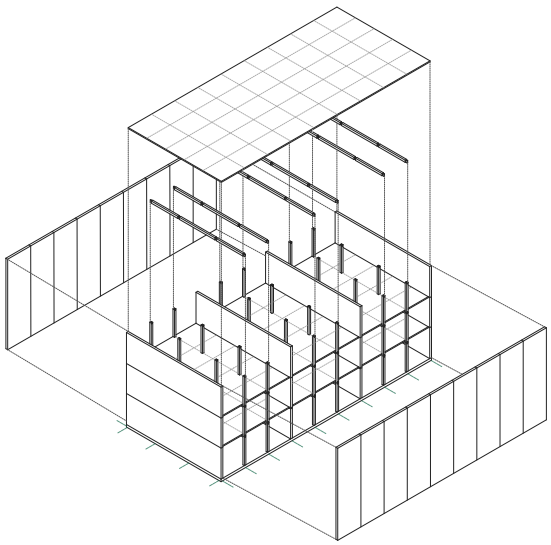

Figure 3: Basic Unit
Figure 4: Assembling the structural elements

These basic units foster the creation of user communities where sound insulation aligns with socio-economic aspects and mutual consideration. In the realm of building policies, it's increasingly recognized that standards and guidelines need revision when they impede sustainability. Therefore, the focus on variability takes precedence. The support structure comprises horizontal timber frame panels and glulam pillars, reinforced by a glulam continuous beam and diagonally doweled board stacking elements, referred to as «Brettstapel», as ceiling. The longitudinal facade features non-load-bearing curtain timber frame panels that are efficiently prefabricated, extending the full height of the facade and reinforcing the structure. (cf. figure 4)

4.3. The design principle

The basic unit's grid relies on a wood panel size of 62.5, determined by parameters for living and working uses, prefabrication criteria, transport dimensions, and assembly. Also the element sizes result from this factors. The design emphasizes sufficiency, efficiency, and consistency in terms of material use and functional variations. The floor area of each usage unit is 110 m², structured only by the four wooden supports and a vertical installation shaft. Its placement is determined by the configuration of the «Brettstapel» ceiling and the alignment of all designed floor plan variations. The central area, designated as the common space, encompasses the largest column-free area. This space is multifunctional, serving as an adaptable cabinet zone while optimizing the even distribution of loads to support an efficiently sized continuous beam. By adding the base unit vertically and horizontally, various typologies have emerged. Two main types have been developed:
Type A is accessible via access balconies located in front of the facade, with an external staircase on the front side. The bracing takes place via the vertical elements of the longitudinal facades.
Type B provides access through internal cross-laminated timber staircases, which also serve the purpose of structural stiffening. My detailed construction focus primarily centered around type B.

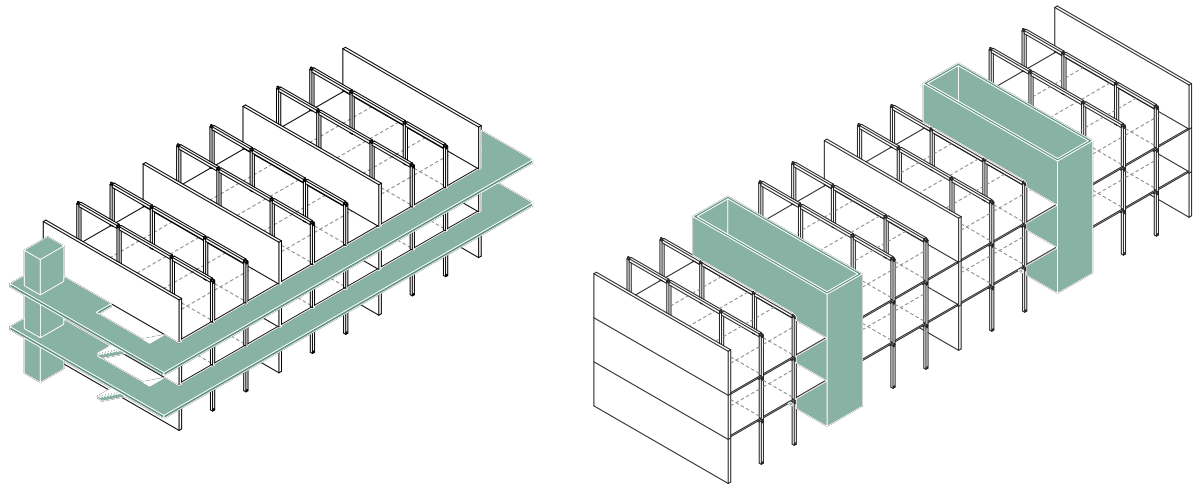

Figure 3: Type A | Type B

4.4. Different execution options

The developed principle is versatile and can be integrated not only as a standalone structure but also to complement existing buildings horizontally or vertically by adapting to the grid. To simplify material usage and detailing, I have specifically tailored this design to fit within building class 3. Expanding the building class would have necessitated additional resource-intensive measures, particularly in areas like fire safety.
In the future, this design principle offers the potential for rooms to be extended outward, allowing individual access via balconies (as in Type A) or balconies as private outdoor space. The rooftop, adorned with lush greenery, offers a communal open space, serving

dual purposes for both solar energy generation and gardening. This approach effectively compensates for the sealed building surface below.
Considering various circular foundation methods such as earth screws, I have chosen for the detailed showcase a straightforward R-concrete base plate due to the height constraints of Building Class 3. Additionally, the non-load-bearing longitudinal timber frame panels are designed with a reversible connection to the supporting structure, enabling the future potential use of photovoltaic elements as part of the facade.

4.5. Two various floor plans

Distinct floor plan typologies highlight different approaches to variability:
The adaptive floor plan (cf. figure 4) allocates space for a cluster apartment, emphasizing the organization of private and communal areas through closet zones. The flexibility allows for easy transitions in usage. In the flexible floor plan (cf. figure 5), zoning of the usage-neutral rooms is achieved through cupboards, shelves, or curtains, providing adaptability to users' needs. Material efficiency is the focal point, particularly in the cluster apartment type, where resource-intensive functions like the bathroom and kitchen are radically minimized.

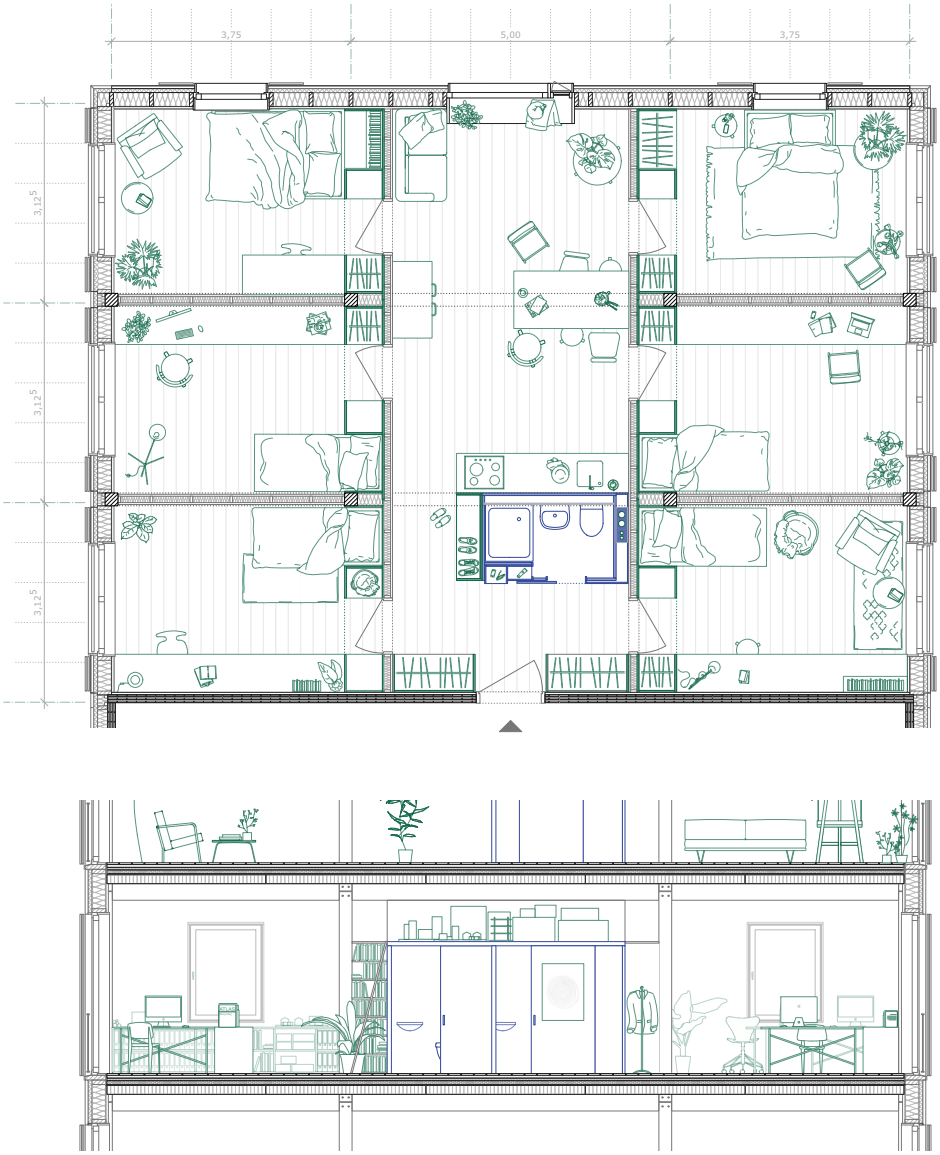

Figure 4: the adaptive floor plan (cluster apartment) | section of the flexible floor plan (open office)

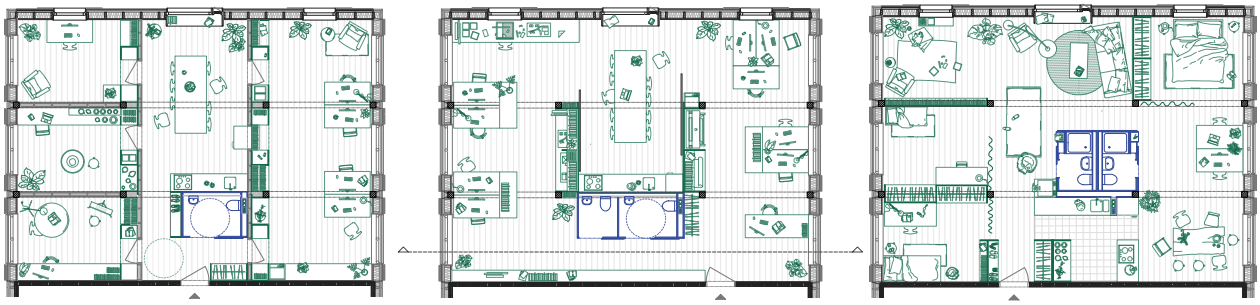

Figure 5: adaptive floor plan (working units) | flexible floor plan (open office) | flexible floor plan (family flat)

4.6. Circular characteristics of the design principle

The circularity of the design principle is rooted in its simplicity and reversible connection, illustrated in Figure 6. Here's how it works:

The vertical load transfer supports feature an innovative end-grain on end-grain connection. These pillars are separated by elastomer supports and are secured to the continuous beam through a traditional carpenter joint known as «Einhälsung» This design avoids transverse compression of the longitudinal fibers by maintaining within the joint a specific distance from the pillar. Additionally, the diagonally doweled «Brettstapel» elements are assembled on top of this structure.
To assess and reaffirm the circular potential of the materials used, I employed the Recycling Atlas. When selecting materials, I carefully considered factors such as durability, sufficiency, and circularity. In addition to wood, hemp, and clay emerged as the primary materials in this eco-conscious design.

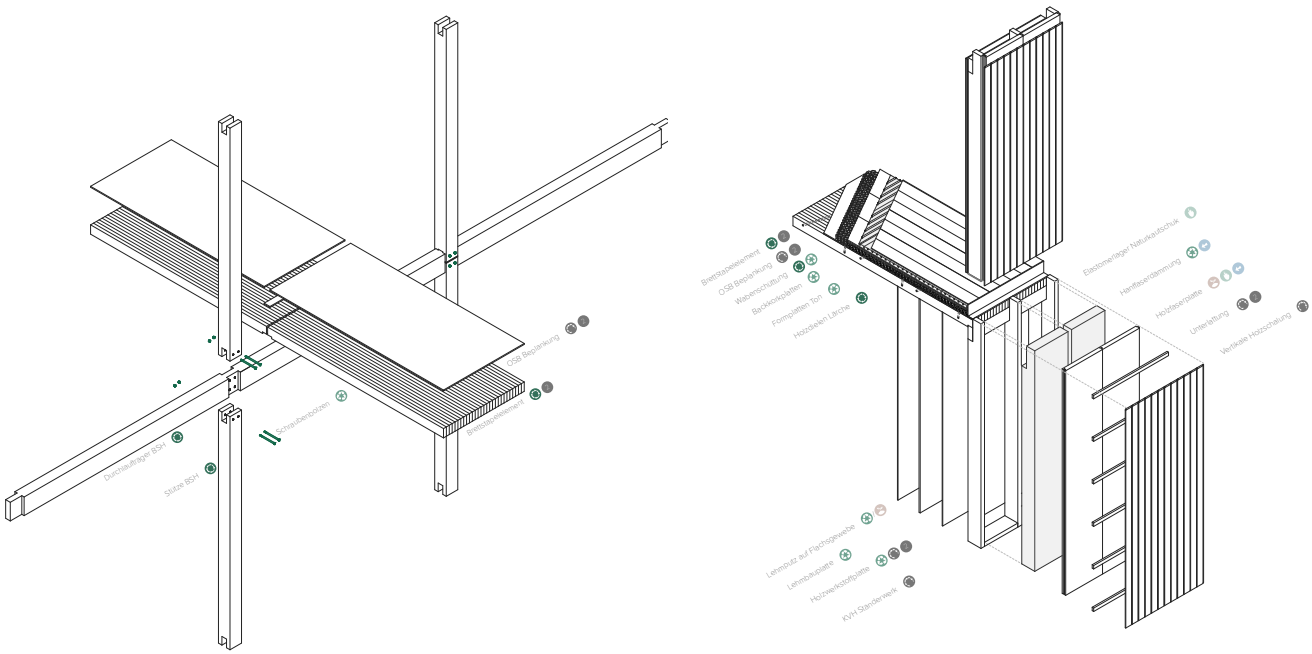

Figure 6: exploded assembly drawing of the reversible joint | exploded section of the load-bearing facade

In staying true to mono-materiality, wooden dowels would be conceivable to secure the joint positions. Since the focus is on reusing the elements instead conventional screw bolts were chosen for their simplicity, economy and reversibility.
The suspended timber frame panels are connected to the supporting structure via screwed wooden laths, featuring removable formwork boards in front of element joints for future accessibility and readability of the facade.
Most connections rely on form-fitting methods secured with wooden dowels or screws, which can be removed even decades later when handled with care and protected from weather. The exception is the weather-exposed screw connection of the facade formwork, which only bears the board's weight and is therefore unlikely complicate to dismantle. Load-bearing horizontal timber frame panels employ continuous stud frames to avoid cross-pressure, positioning the studs of storey-high elements with end-grain surfaces directly atop one another. The top plate, referred to as «Rähm», is rotated by 90° and provides linear support for the ceiling elements. (cf. figure 6, section)

5. Conclusion and foresight

5.1. Circular potential of the design principle

Using the Urban Mining Index, a digital tool from Prof. Dr. Anja Rosen, the calculation illustrates the high circular potential of the design principle (the urban mining indicator) at 70%. (cf. figure 7)
The deviation from 100% stems from open material cycles, such as the downcycling of R-concrete floor slabs and window glass. Additionally, the circular economy is yet to be fully established, leading to insufficient supplies of secondary raw materials for some materials. A closed cycle for materials like clay as a building material could be viable in the future once the circular economy and supporting infrastructure is better established.

Figure 7: results of the Urban-Mining-Index ©2021 Urban Mining Index | Prof. Dr. Anja Rosen

5.2. The role of timber

The construction and design principle developed here demonstrates how timber can play a central role in a circular building economy. The cascade potential of Timber, already being a sustainable regrowing material, offers maximizing the use of our existing timber resources and forests. This approach not only safeguards our sustainable forestry from overexploitation but also allows timber buildings to replace conventional structures and thus compensate carbon dioxide. While my work on joint solutions raised numerous new questions, I am encouraged by the growing expertise in universities and the potential for research and Ph.D. programs. Although there is much work ahead, interdisciplinary collaboration within the timber building industry, drawing expertise from all stakeholders in various fields, will gradually lead us towards a future circular timber economy.

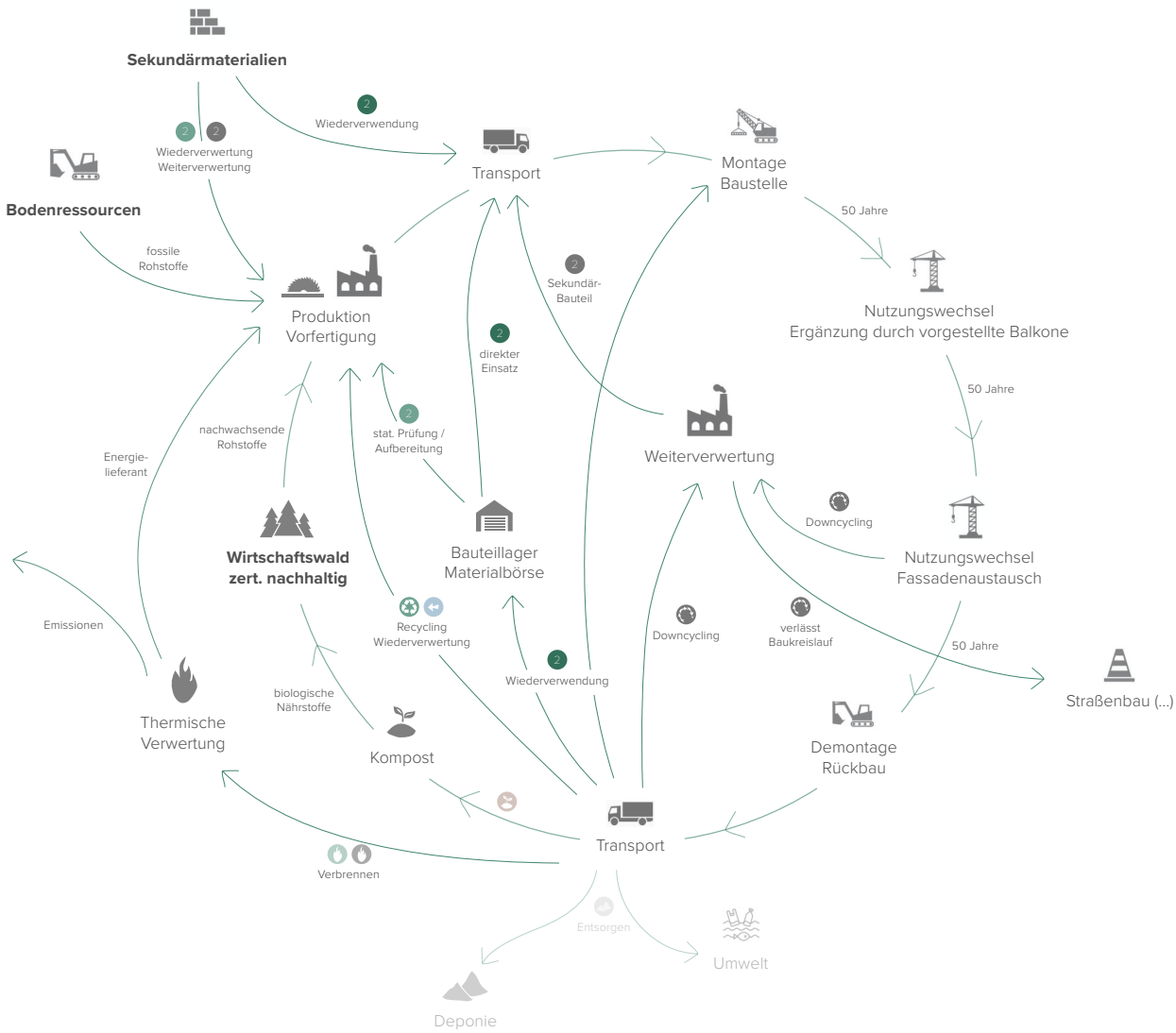

Figure 8: circular cycle of the developed construction system

5.3. How will we live together?

The theme of the Architecture Biennale 2021 in Venice raises essential questions about our future. The way we plan and construct today significantly impacts our lives tomorrow and our ability to create circularity in our built environment. It's imperative to recognize that major social changes, possibly even upheavals, could occur during the long lifespan of well-conceived and constructed buildings. To adapt quickly to the evolving needs of communal living, we must transition from isolated apartments and small family units towards intergenerational living, shared apartments, or cluster typologies. The synergies of shared living present social, economic, and structural opportunities that may become vital for our survival. It's crucial to design buildings today that can flexibly adapt tomorrow, promoting communal living and quality coexistence.

Figure 9: interior vista - How will we live together?

1. Sources of figures

fig. 1 Umweltbundesamt, 2019, https://www.umweltbundesamt.de/altholz#verwertung-und-pro-duktion-in-deutschland, Abrufdatum: 22.09.2023

fig. 2 Cascade usage of timber, Höglmeier et al., 2016

fig. 7 ©2021 Urban Mining Index | Prof. Dr. Anja Rosen

fig. 9 Poster Biennale di Architettura, Studio Omnivorous, 2021

References

[1] Herzog, Thomas; Natterer, Julius, Schweitzer, Roland; Volz, Michael; Winter, Wolfgang: Holzbau Atlas. 4. Auflage, Edition Detail, München 2003, Seite 49

[2] Vortrag Dr. Michael Risse (Lehrstuhl für Holzwissenschaft, TUM), "Auf ins neue Holzzeitalter. Wie kostbar ist Holz?", evang. Akademie Tutzing, am 05.02.2023

[3] wie [2]

[4] ZHAW Institut Konstruktives Entwerfen (Hrsg.); Stricker, Eva; Brandi, Guido; Sondereger, Andreas (ua.): Bauteile wiederverwenden - ein Kompendium zum zirkulären Bauen. Zürich 2021, Seite 95

[5] wie [4], Seite 96

[6] wie [4], Seite 100

branntneu.
Neighbourhood development and redensification in timber construction on the Branntweinareal in Munich

Anna-Maria Brendel
Technical University of Munich
Chair of Architecture and Timber Construction
Munich, Germany

branntneu.

1. Introduction

The development of conversion areas in urban spaces presents an opportunity for resource-efficient development through the analysis of existing structures and the promotion of sustainable construction methods. This encompasses the reuse of existing buildings, reduction of demolition waste and the use of eco-friendly building materials. A resource-efficient approach can offer economic advantages and reduce the environmental impact of urban development. At the same time, these areas can shape the distinctive identity of a neighbourhood or urban landscape.
Examples from Munich illustrate how conversion areas and former industrial sites are often gradually replaced by dense, investor-driven architecture that frequently neglects human needs and urban scale. Liveable neighbourhoods, however, are key to creating people-centric urban development. This includes promoting social diversity, avoiding uniform land use and offering a wide range of housing options.
Modern timber construction in urban settings offers a sustainable and aesthetically pleasing solution with shorter and more precise construction periods, thanks to a high degree of prefabrication. This not only accelerates the construction process but also reduces costs and minimizes disturbances to residents. It contributes to realizing vibrant and liveable urban neighbourhoods more swiftly and enhances the appeal of modern timber construction in urban areas. The objective is to make these potentials visible, both for urban planners and the general public. This can be achieved through education, information campaigns, and pilot projects in modern timber construction to raise awareness for the benefits of this sustainable approach and promote its implementation in urban development.

Figure 1: Hirschgarten Munich © Leon Ambaum

Figure 2: Entrance Branntweinareal Munich

2. Presentation Branntweinareal Munich

One of Munich's last remaining former industrial areas is the site of the former Federal Monopoly Administration for Spirits, situated south of the Eastern railway track at Leuchtenbergring. Presently, there are no specific plans for the repurposing of the existing facilities. Therefore, the city is contemplating a demolition plan, followed by subsequent development and construction. This course of action often accompanies a loss of identity, as has been observed in numerous neighbourhood development projects on former conversion sites.
The roughly two-hectare area on Leuchtenbergring was transformed into an alcohol production factory at the beginning of the 20th century. At that time, the planning area was located outside of Munich city boundaries, but it was already connected to the railway and public transport networks. Over the course of the past century, the area underwent gradual expansion with the construction of buildings, ultimately evolving into the complex it is today. A significant structural transformation occurred when the main circular road was built, resulting in the division of the property by an underpass in the 1950s. The construction of the factory tower in 1976 marked the architectural completion. This tower, standing at a height of over 25 meters, is now a protected heritage site and serves as a prominent landmark, highly visible from the railway tracks.

The area is situated within a highly diverse urban context. The existing buildings on the property were analysed with respect to their location, structural composition, building materials, architectural aesthetics, and potential for reuse. The buildings along the railway line, including halls, a pagoda, silos, and the «Apparatehaus», met the analysis criteria set and have therefore been preserved and integrated into the urban planning process.

3. Concept

3.1. Urban Development Concept

The urban design envisions a concept that allocates adequate spaces for both the pre-existing and newly constructed buildings. The spaces between these structures forms the new centrepiece of the area. It is accessed via the factory gate, which spans between the new buildings and opens up the Branntweinareal to the Berg am Laim district for the first time and creates accessibility. This threshold, situated between the existing and new buildings, establishes a new urban zone featuring diverse gathering places tailored to accommodate various user groups.
The vertical development of the two new buildings aligns with the existing urban fabric, integrating the area into the neighbourhood. The urban landmarks consist of the «Apparatehaus» and the chimney, which are clearly visible from the railway track. The spaces between the buildings create public and semi-public areas of varying scales for the user groups. Furthermore, synergies emerge between the existing and new structures.

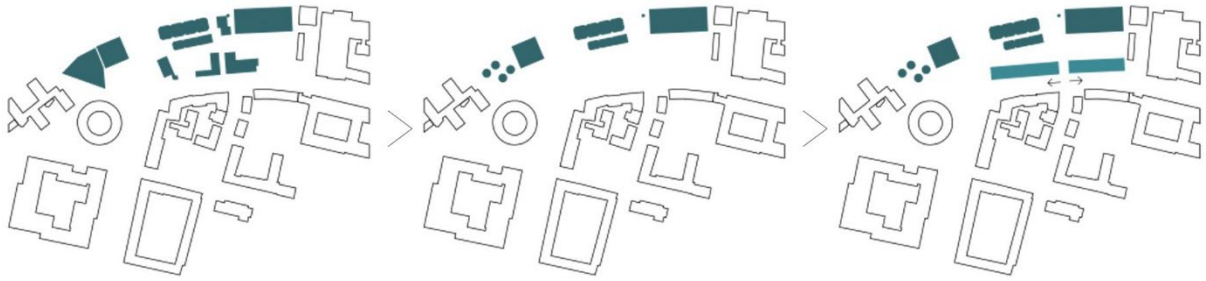

Figure 3: Urban planning analysis

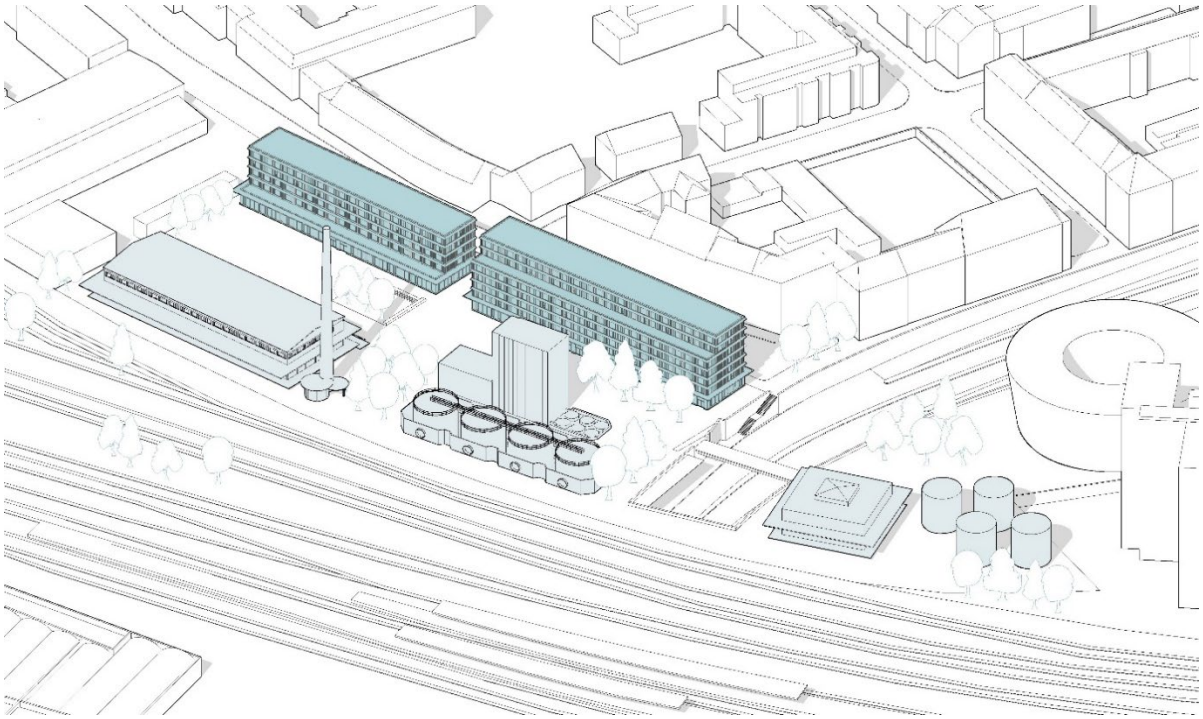

Figure 4: Axonometry Branntweinareal

3.2. Usage Concept

The objective is to make versatile use of the area, keeping it dynamic and vibrant through a range of spatial programs. Rather than limiting uses, the aim is to strengthen them and promote interaction to generate synergies.
The area will be allocated to three new user groups, all connected to the central main square. In addition to public and cultural functions, the new constructions will address the need for residential space. A public use includes a vocational school specializing in media, print, and design, for which the city of Munich is currently seeking a suitable location. Furthermore, a dormitory will be connected to the school to provide an opportunity for students from outside the area to reside there. Space will also be designated for artists, small businesses, and social gathering areas within the existing buildings in the southeast. The positioning of these structures in relation to one another creates a sequence of squares and outdoor spaces that can be activated flexibly.

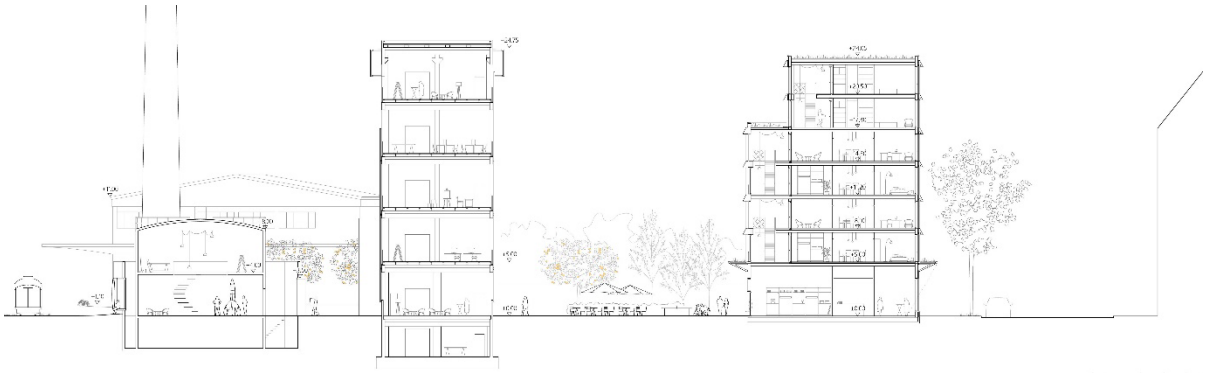

Figure 5: cross-section residential building

4. Design

The design includes a conceptual plan for the redesign of all existing buildings and an appropriate use concept for them in combination with the two new buildings. On the ground floors, alongside the access areas for the upper levels, there are substantial and deep spaces tailored for more public uses. In response to the public character of these ground-level spaces, the primary aim was to establish communal areas for the residents on the upper levels. To achieve this, two floors are connected and accessed through an atrium in the northern part of the buildings.

4.1. Organisation Residential Building

The residential building block in the southwest rises to a height of seven stories. On the ground floor, in addition to the circulation areas for the residential building above, bicycle and laundry rooms and a community workshop for the residents, there are six shops, which are oriented towards the central main square towards. This design ensures that the ground floor remains a vibrant public space, effectively interacting with the outdoor environment.
Above are six upper floors offering a variety of living typologies ranging from one-room studios to five-room flats. Every two floors share a double-height space, thoughtfully designed to introduce abundant natural light through the northern façade. The residential building's concept promotes the sharing of spaces within the community. These light-filled areas serve as hubs for communal and recreational activities, housing shared facilities like expansive kitchens, children's play areas, a fitness room, a library, and a co-working space. This approach allows the housing floor plans to be reduced to private living while reserving shared spaces for coordinated use by the residents.
The first four upper levels feature four-bedroom apartments and flexible cluster units that can be adjoined as needed. The upper two levels are one grid interval less deep, accommodating smaller residential units. The diverse array of apartment types provides residents with the flexibility to change residences within the building according to their evolving needs and life circumstances, all while remaining a part of the building's community.

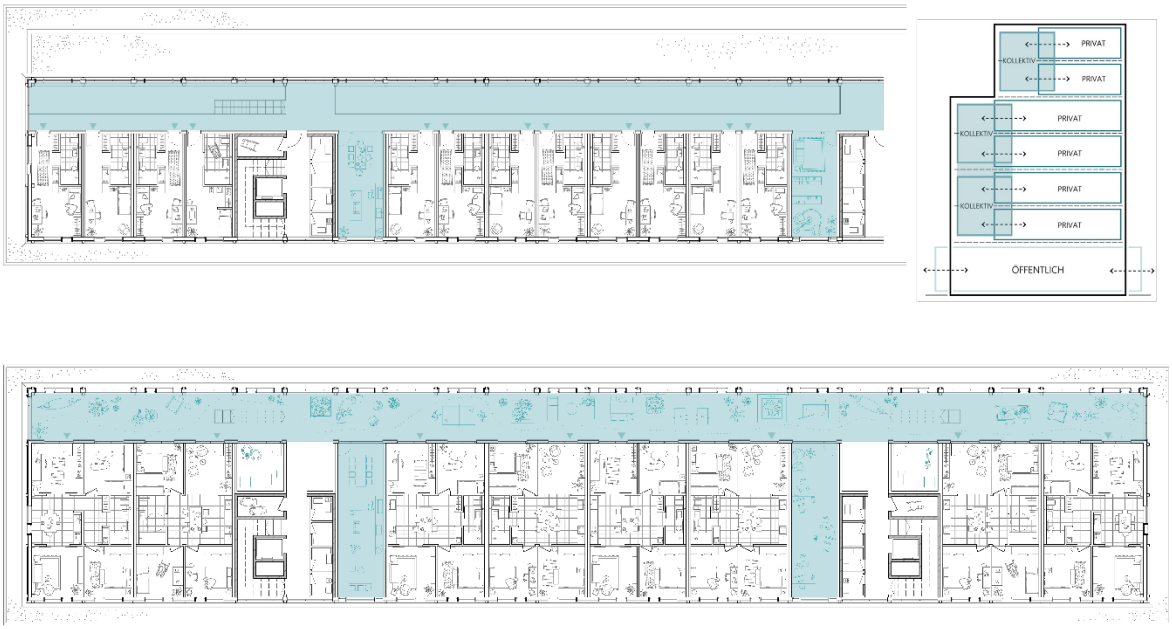

Figure 6: Floor plans residential building / pictogram

4.2. Organisation School Building

The planned vocational school for media, print, and design consists of two buildings that enclose a central courtyard. In addition to fulfilling the conventional spatial requirements of a school, this vocational institution requires workshops and laboratories for practical, hands-on instruction within the respective disciplines. The existing hall, featuring a two-story column-free interior, provides an ideal space for the arrangement of these workshops and laboratories. Furthermore, students are provided with dedicated workstations that remain accessible to them beyond regular class hours.
On the other hand, the newly designed block accommodates the rooms needed for the typical daily activities for teaching and the staff. Here, the ground floor serves as a publicly accessible area for students, incorporating exhibition spaces, an auditorium, and the student council offices. On the first two upper levels, a total of 10 seminar rooms provide room for the regular instructional activities, and their flexible configurations are made possible using mobile partitions.
Above the school, a dormitory for 28 students is planned, addressing the prevailing shortage of accommodations for students commuting from outside the immediate area. These apartments are generously sized at 26.00 square meters and provide students with the possibility of longer stays. Each floor is connected via a light filled communal space and an adjoining gallery, offering spacious shared areas for students. In addition, two communal kitchens are connected to the light room on each floor.
The courtyard between the two buildings is thoughtfully designed with a sports field and a south-facing staircase, ensuring a high-quality gathering place. It also seamlessly connects to the newly established neighbourhood square in the west, thereby enhancing the overall environment and cohesiveness between existing and new architectural elements.

4.3. Facade and Design

The basic principle of the building structure is also clearly visible in the façade. The ground floor is notable for its very urban façade and is separated from the storeys above by a surrounding canopy. This canopy forms a design homage to the canopies of the existing buildings and blends seamlessly into the site.
On the upper floors, the facade design highlights the wooden structure. Despite a high degree of repetition, the facade remains dynamic due to interruptions created by the staircases and individual adaptations by the residents. The two-story light rooms are also evident in the facade. Transparent glass elements allow direct natural light and views, while the rest of the facade is constructed from translucent polycarbonate.

The facade is a prefabricated wooden facade with architecturally detailed fire-resistant elements that also draw inspiration from the existing buildings. These elements wrap around the building as horizontal bands, adding visual structure to the facade. In addition to their fire-resistant function, they house the sunshades. Since the large fire-resistant elements are expected to weather irregularly, the facade wood is not left in its natural state but is instead pre-stained.

Figure 7: Facade section / elevation

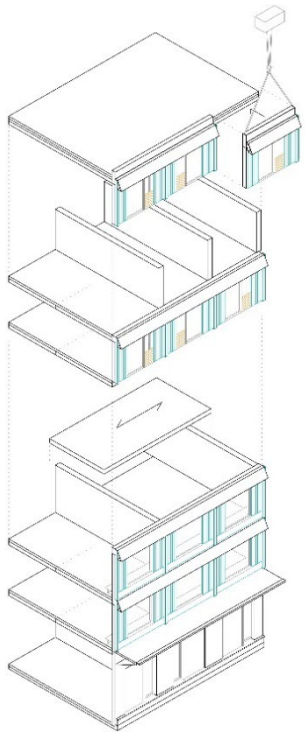

Figure 8: pictogram assembly

5. Construction / Assembly

The design is conceived as a bulkhead construction, based on a main structural grid of 7.50 meters. This grid can face the structural requirements of all uses (residential, school, and public retail areas) and provides flexible use options for the future. Load-bearing two-shell frame walls, in combination with cross-laminated timber (CLT) ceilings, form the structural system orthogonally to the facade. The design combines the advantages of CLT with timber frame construction and optimizes wood consumption in times of significantly increased timber prices. The frame walls also meet the acoustic requirements between individual units. Given the length of the building, the wooden structure is braced using two reinforced concrete cores containing staircases and elevators. Furthermore, the floor plan allows a direct readability of the installation areas for bathrooms and kitchens through a compact planning, which has a high degree of prefabrication.
The design utilizes cross-laminated timber (CLT) ceilings, which run parallel to the facade, offering independent and unrestricted options for facade design and installation, separate from the primary structural framework. In the ceiling area, the facade elements, designed on a 3.75-meter grid, are anchored in a rearward position. The facade can be fully prefabricated off-site and transported to the construction site for assembly. Both the residential and school buildings are based on the same structural and construction principles, taking advantage of prefabrication in timber construction.
The process of erecting floors follows a consistent approach. First, bulkhead-like frame walls are assembled, and then the spanning CLT ceilings are placed. The factory-prefabricated exterior wall elements with windows, sunshade and wooden façade are installed in front of the ceiling panels in a sound-insulated manner.

6. Conclusion

The conversion of old industrial sites and the careful analysis of their typological legacies offer considerable urban planning potential, especially with regard to contemporary building requirements. Combined with modern timber construction methods, they enable a flexible and resource-efficient planning process that is oriented to current architectural standards. Incorporating the structural advantages of timber construction into the design process at an early stage enables specific solutions to urban planning challenges. The fusion of historic industrial buildings with contemporary architecture not only enhances neighbourhood development, but also contributes significantly to the diversity and sustainability of urban spaces and thus promotes liveable and future-oriented urban development.

Figure 9: Rendering «Werkstor»

Vertrieb FORUM **HOLZBAU**
Bahnhofplatz 1, 2502 Biel/Bienne, Schweiz
T +41 32 327 20 00
info@forum-holzbau.com
www.forum-holzbau.com

ISBN 978-3-906226-60-6